Research Square

Preprints are preliminary reports that have not undergone peer review.
They should not be considered conclusive, used to inform clinical practice,
or referenced by the media as validated information.

Chromosomal fusions shaped karyotype evolution in Moraceae with only the γ whole-genome duplication

Qiming Zhou

zhouqiming6324@163.com

Southwest university https://orcid.org/0009-0002-7731-5003

Ziang Li

Southwest University

Jiacheng Li

Southwest University

Yaning Liu

Southwest University

Jiali Qiu

Southwest University

Jianglian Yuan

Southwest University

Zhengang Li

Yunnan Academy of Agricultural Sciences

Song Chen

Yunnan Academy of Agricultural Sciences

Yahui Xuan

Southwest University

Ningjia He

Southwest University

Research Article

Keywords: polyploidization, ancestral karyotype, chromosomal fusion, Moraceae, Morus

Posted Date: November 24th, 2026

DOI: https://doi.org/10.21203/rs.3.rs-11818721/v1

License: This work is licensed under a Creative Commons Attribution 4.0 International License.
Read Full License

Additional Declarations: The authors declare no competing interests.

Chromosomal fusions shaped karyotype evolution in Moraceae with only the γ whole-genome duplication

Qiming Zhou [1†], Ziang Li [1†], Jiacheng Li [1], Yaning Liu [1], Jiali Qiu [1], Jianglian Yuan [1], Zhengang Li [2], Song Chen [2], Yahui Xuan [1*], Ningjia He [1*]

[1] State Key Laboratory of Resource Insects, Southwest University, Beibei, Chongqing, 400715, China

[2] Sericulture and Apiculture Research Institute, Yunnan Academy of Agricultural Sciences, Mengzi, Yunnan, 661101, China

[†] These authors contributed equally to this work.

*Corresponding author: Yahui Xuan, E-mail: xuanyahui@swu.edu.cn; Tel: +86-23-6825-1615; Ningjia He, E-mail: hejia@swu.edu.cn; Tel: +86-23-6825-0797; Fax: +86-23-6825-1128

Abstract

Polyploidization is a core driver of terrestrial plant speciation and adaptive evolution. Post-polyploid diploidization coupled with chromosomal rearrangement shapes karyotype stability and lineage diversification in existing plants. However, how chromosomal rearrangements drive karyotype evolution in paleopolyploids remains fragmentary. Most Moraceae species have experienced only a single ancient whole-genome duplication (WGD) yet exhibit extensive variation in ploidy and basic chromosome number, making Moraceae an ideal model for investigating chromosomal rearrangements during the evolution of paleopolyploids. Here, we developed oligo probes targeting conserved chromosomal regions in *Morus* to dissect the karyotype evolution histories in Moraceae. High-resolution oligo painting and rDNA mapping revealed the distinctive polyploid nature of *Morus*. Co-localization of centromeric and telomeric sequences uncovered rapid karyotype evolution in five *Morus* species. Synteny analyses and the reconstructed ancestral Moraceae karyotype identified chromosome fusion as the core driver of basic chromosome number reduction in Moraceae. *Morus notabilis* (2n=2x=12) represents the most

"advanced" karyotype shaped by eight end-to-end joining events. Our results indicate that chromosome fusion-mediated karyotypic evolution has driven both speciation and karyotypic diversification within Moraceae, thereby offering an excellent framework for understanding karyotype evolution in paleopolyploid plant lineages.

Keywords: polyploidization; ancestral karyotype; chromosomal fusion; Moraceae; *Morus*

1 Introduction

Polyploidization is a fundamental mechanism driving plant evolution, speciation, and adaptive radiation [1,2]. Unlike animals, plants exhibit a remarkable tolerance to whole-genome duplication (WGD) [3,4]. Notable examples include allotetraploid cotton, allohexaploid wheat, and sugarcane with higher ploidy levels [5-8]. The genetic redundancy resulting from genome duplication provides a rich substrate for gene mutation, functional divergence, and chromosomal rearrangement, thereby significantly enhancing plant environmental adaptability, colonization ability, and phenotypic plasticity [9-12]. For instance, genome doubling significantly improves salt tolerance in *Citrus* and *Poncirus* [13]. In *Gossypium hirsutum*, polyploidization drives functional divergence among homologous genes of *GhCIPK6* under drought stress [14]. Consequently, polyploidization is regarded as a key factor in the rise of angiosperms and their dominance as the major plant group on Earth [15].

Despite conferring genetic redundancy and adaptive advantages, polyploidization often leads to genomic instability, meiotic irregularities, and fertility decline in neopolyploids [16,17]. Over time, diploidization, encompassing both structural and functional aspects, gradually restores polyploids to a state resembling native diploids in karyotype, meiotic behavior, and gene expression regulation [18-20]. A well-known case is hexaploid (bread) wheat and tetraploid (pasta) wheat, whose meiotic progression displays typical diploid characteristics mediated by the *Ph1* gene [21]. Meanwhile, a possible and important concomitant process in polyploid is chromosome number reduction. Through chromosomal rearrangements and centromere fusion or inactivation, chromosome numbers were eventually reduced [22-24]. For example, *Zea mays* and *Brachypodium distachyon* underwent whole genome doubling and subsequently reduced their basic chromosome numbers via chromosome fusion [25,26]. Chromosome number reduction further

alleviates the pressure of chromosome pairing during meiosis [27]. These processes enable the stable population persistence of neopolyploids.

The family Moraceae comprises approximately 48 genera and 1,140 species, characterized by high genetic diversity [28]. These species exhibit extensive variation in basic chromosome numbers (ranging from 6 to 28) [29-33], chromosome counts (from 12 to 308) [34], and ploidy levels (from 2x to 22x) [29,34,35]. The γ-WGD represents an ancient whole-genome triplication shared by eudicots, whereas the α- and β-WGDs are younger lineage-specific WGD documented in certain eudicot lineages such as *Brassicaceae*. *Morus notabilis* (2n=2x=12) and *Broussonetia papyrifera* (2n=2x=26) have not undergone the recent α- or β-WGD events and only share the ancient γ-WGD [29,30]. The diversification of their basic chromosome numbers was further driven by a series of complex chromosomal rearrangements [30,36]. In contrast, the genus *Artocarpus* (x=28) experienced a lineage-specific WGD after its divergence from *Morus*, which directly resulting in the doubling of basic chromosome number [31]. Collectively, the extensive divergence in ploidy and basic chromosome numbers among Moraceae members, makes this family an ideal model for investigating the evolutionary processes of shifts in basic chromosome numbers after γ-WGD.

Within Moraceae, the genus *Morus* exhibits the widest variation in ploidy levels (2x, 3x, 4x, 5x, 6x, 9x, 22x) and possesses two highly divergent basic chromosome numbers (x = 6 and x = 14) [29,34,36,37]. *M. notabilis*, which originated from drastic chromosomal rearrangements, serves as an excellent model plant for understanding dynamic changes in basic chromosome numbers [36]. In this study, we developed a set of oligonucleotide painting (oligo-painting) probes targeting conserved chromosomal regions of *Morus* using genomes of *M. alba* and *M. notabilis*. High-resolution oligo-painting revealed the initial polyploid nature of *Morus*. Colocalization of rDNAs, centromeres, telomeres, and oligo probes uncovered rapidly evolving centromeric regions and potential chromosomal evolutionary events in *Morus*. Moreover, genomic collinearity analysis and the reconstructed ancestral Moraceae karyotype systematically revealed the complex evolutionary trajectory of Moraceae. We found that chromosomal fusions reduced the basic chromosome number of Moraceae species, thereby serving as a core driver of their evolution and karyotypic diversification. Using Moraceae as an example, this study examines polyploidization and associated changes in basic chromosome numbers in paleopolyploid plants that have experienced only

the γ-WGD. This work provides a reliable reference for understanding these evolutionary dynamics.

2 Results

2.1 Development of oligo-painting probes in *Morus*

To develop a set of chromosome-conserved-region painting probes in *Morus*, single-copy oligos were computationally identified based on the 14 pseudomolecules of the *M. alba* genome using Chorus2 [38,39]. The lengths of the *M. alba* pseudomolecules ranged from 13.98 Mb (Chr14) to 64.90 Mb (Chr1) (Supplementary Table 1). To obtain highly conserved oligos, 45 nt sequences on chromosomes 3–14 were screened with the parameters -l 45 -homology 98 -step 5. Owing to the extremely high abundance of repetitive sequences on *Morus* chromosomes 1 and 2, the homology threshold was lowered to 75 and 80, respectively, to recover a sufficient number of valid oligos. The preliminarily selected oligos were further filtered to remove putative repetitive sequences, yielding the final oligo library.

In total, 459,405 single-copy oligos were identified for *M. alba*, ranging from 23,848 (Chr13) to 58,844 (Chr1) (Supplementary Table 1 and Supplementary Data). The average oligo density of the 14 chromosomes ranged from 0.91 oligos per kilobase (Chr1) to 1.95 oligos per kilobase (Chr11) (Supplementary Table 1). The oligos covered most regions of each *M. alba* chromosome (Figure 1a). However, relatively low densities of single-copy oligos were observed in certain chromosomal regions, particularly in the putative pericentromeric regions of chromosomes 1 and 2 (Figure 1a). Consequently, painting signals in these repeat-rich chromosomal regions could not be detected in subsequent experiments.

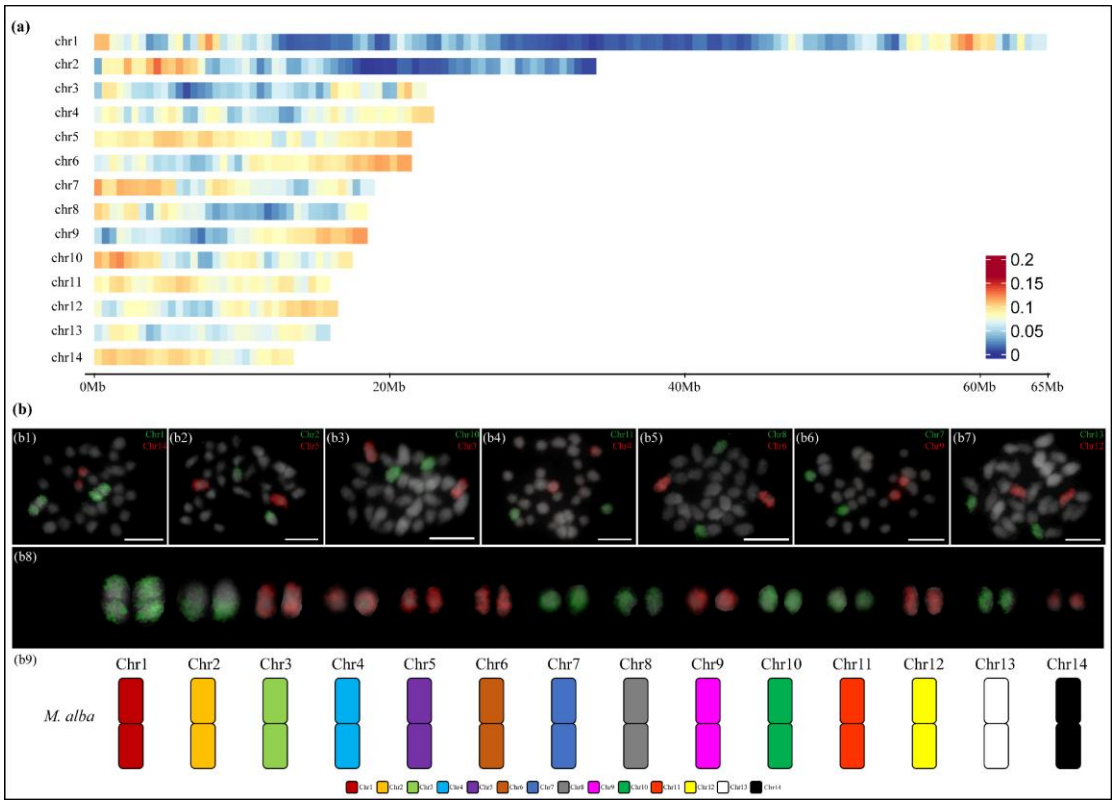

Figure1. Development of chromosome-specific oligo-painting probes in *M. alba* (2n=2x=28). (a) The 14 chromosomes of *M. alba* were divided into 500-kb windows, and the number of oligos per window was calculated. The distribution of oligo abundance is shown in a heatmap. (b) Oligo-painting experiments were performed on *M. alba* using 14 chromosome-specific painting probes. The following probe combinations were applied: Chr1 and Chr14 (b1); Chr2 and Chr5 (b2); Chr10 and Chr3 (b3); Chr11 and Chr4 (b4); Chr8 and Chr6 (b5); Chr7 and Chr9 (b6); and Chr13 and Chr12 (b7). (b8) Chromosomes labeled by oligo-painting were digitally excised from the images shown in panels b1–b7. (b9) Ideogram illustrating chromosomes 1–14 of *M. alba*. Scale bars represent 5 μm.

2.2 Chromosome-specific oligo-painting in *M. alba*

Oligo-painting probes were labeled with either FAM (green) or TAMRA (red). The 14 oligo-painting probes (Chr1–Chr14) correspond to pseudomolecules 1 to 14 of the *M. alba* genome. To evaluate probe quality, pairs of probes were hybridized to metaphase chromosome preparations of *M. alba*. After seven rounds of oligo-painting, all 14 chromosomes were unambiguously identified (Figure 1b). All probes generated bright and specific fluorescent signals on homologous chromosome pairs, confirming their ability to specifically identify all conserved chromosomal regions across the genus *Morus*.

The 28 FISH-labeled chromosomes were digitally excised from Figure 1 b1–b7, arranged according to short arm–centromere–long arm (Figure 1b8), and visualized (Figure 1b9). The results showed that the size of signal gaps in the pericentromeric regions varied considerably among chromosomes. Probes for chromosomes 3–14 produced fluorescent signals that evenly covered the entire chromosomes. In contrast, signal gaps were observed on chromosomes 1 and 2, with the most prominent gap in the pericentromeric region of chromosome 1 (Fig. 1b8). Moreover, no interchromosomal rearrangements were observed, supporting the accuracy of the genome assembly.

2.3 Oligo-painting reveals a distinct karyotype in *M. notabilis*

M. notabilis possesses the lowest chromosome number within the genus *Morus*, a feature attributed to extensive chromosomal rearrangements [36]. In the present study, all painting probes generated bright and distinct signals on each *M. notabilis* chromosomal regions (Figure 2a-d). Consistent with the inferred synteny, *M. notabilis* results from drastic chromosomal rearrangements (Figure 2f). Specifically, four probes(Chr9, Chr7, Chr4, and Chr11) collectively constituted Mn-Chr1 (Figure 2a). Similarly, Mn-Chr 2-4 each corresponded to multiple probes (Fig. 2b-d). By contrast, Mn-Chr 5-6 corresponded to the *M. alba* Chr1 and Chr8 probes, respectively. Notably, uniform oligo-painting signals covered all chromosomes without prominent detectable signal gaps (Figure 2e).

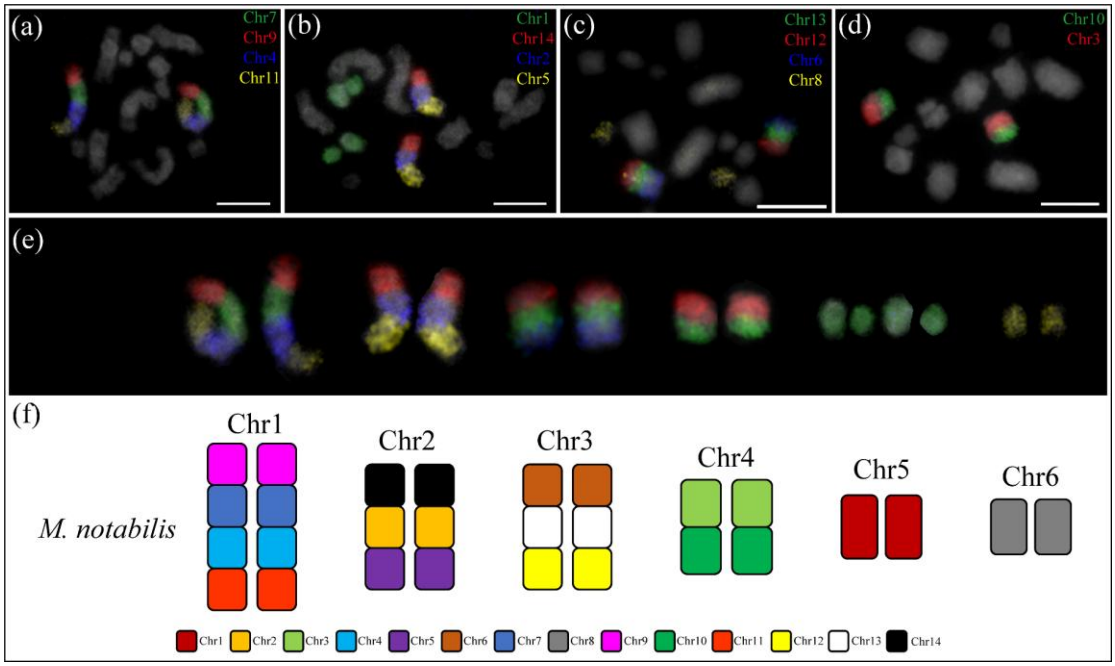

Figure 2. Oligo-painting analysis of *M. notabilis* (2n=2x=12) using chromosome painting probes.

The following probe combinations were applied: Chr7, Chr9, Chr4, and Chr11 (a); Chr1, Chr14, Chr2, and Chr5 (b); Chr13, Chr12, Chr6, and Chr8 (c); Chr10 and Chr3 (d). (e) Chromosomes labeled by oligo-painting were digitally excised from the images shown in panels a-d. (f) Ideogram illustrating Mn-Chr 1-6. Scale bars represent 5 μm.

2.4 Cross-species painting reveals conserved chromosomal synteny among three other *Morus* species

We further investigated chromosomal synteny in additional *Morus* species. *M. laevigata* (2n=2x=28), *M. wittiorum* (2n=4x=56), and *M. cathayana* (2n=6x=84) were selected based on morphological and cytological classification [34,40]. Oligo-painting analysis revealed that all probes generated clear painting signals in the three additional tested species (Figure 3 and Supplementary Figures 1-2). Notably, the number of homologous copies retained per chromosome in each species was consistent with its ploidy level. Specifically, *M. wittiorum* and *M. cathayana* possessed four and six homologous copies, respectively (Supplementary Figures 1h-2h). Meanwhile, no evident interchromosomal translocations were detected in any of three tested species, indicating that the relevant subgenomes remain highly conserved across these species during the polyploidization in *Morus* (Supplementary Figures 1-2 (h-i)). However, signal gaps were detected in the putative pericentromeric regions of several chromosomes across the three species, with the most prominent gaps observed on chromosomes 1, 2, and 3 of *M. laevigata* (Figure 3h).

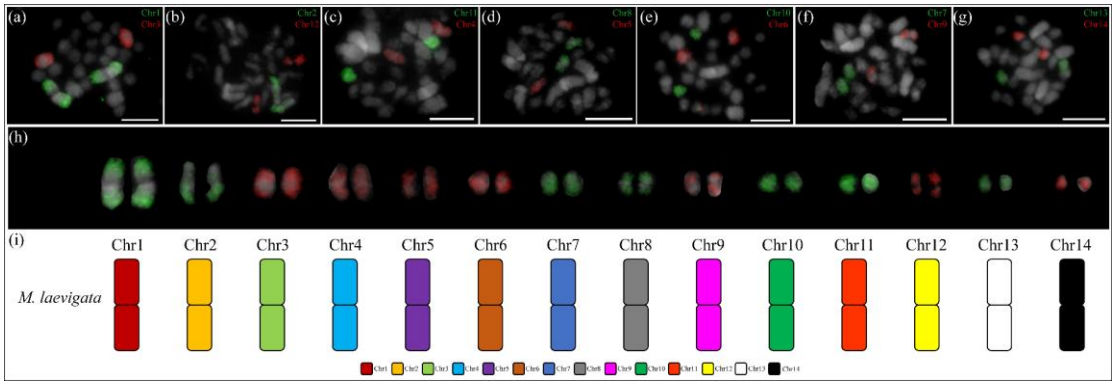

Figure 3. Oligo-painting analysis of *M. laevigata* (2n=2x=28) using chromosome painting probes. The following probe combinations were applied: Chr1 and Chr3 (a); Chr2 and Chr12 (b); Chr11 and

Chr4 (c); Chr8 and Chr5 (d); Chr10 and Chr6 (e); Chr7 and Chr9 (f); and Chr13 and Chr14 (g). (h) Chromosomes labeled by oligo-painting were digitally excised from the images shown in panels a-d. (i) Ideogram illustrating chromosomes 1–14 of *M. laevigata*. Scale bars represent 5 μm.

2.5 Highly conserved ribosomal DNA loci in *Morus*

The physical localization of ribosomal DNA (rDNA)is an important cytogenetic feature widely used for chromosome identification in plants [41-43]. Therefore, we performed sequential FISH with 25S rDNA, 5S rDNA, and oligo-painting probes in the five aforementioned *Morus* species to assess the evolutionary conservation of rDNA chromosomal positions.

Sequential FISH precisely identified the chromosomes carrying rDNA loci (Figure 4). All Morus species shared a conserved rDNA localization pattern: 25S rDNA co-localized with the Chr1 painting probe and 5S rDNA co-localized with the Chr3 painting probe. Specifically, in *Morus* species with x=14, 25S and 5S rDNA were located on chromosomes 1 and 3, respectively (Figure 4b-4e). In *M. notabilis* (x=6), they were located on Mn-Chr5 and Mn-Chr 4, respectively (Figure 4a). The 25S rDNA exhibited signal bands of comparable intensity across all *Morus* species. In contrast, variable fluorescence intensities of 5S rDNA were detected in the high-ploidy species (*M. wittiorum* and *M. cathayana*), and the signals was even lost in *M. cathayana* (Figure 5). In addition, the 25S rDNA locus filled the signal gaps of the Chr1 painting probe in almost *Morus* species. Notably, distinct signal gaps were still observed on chromosome 1 of *M. laevigata*, as well as on one homolog of chromosome 3 in *M. laevigata* (Figure 4c).

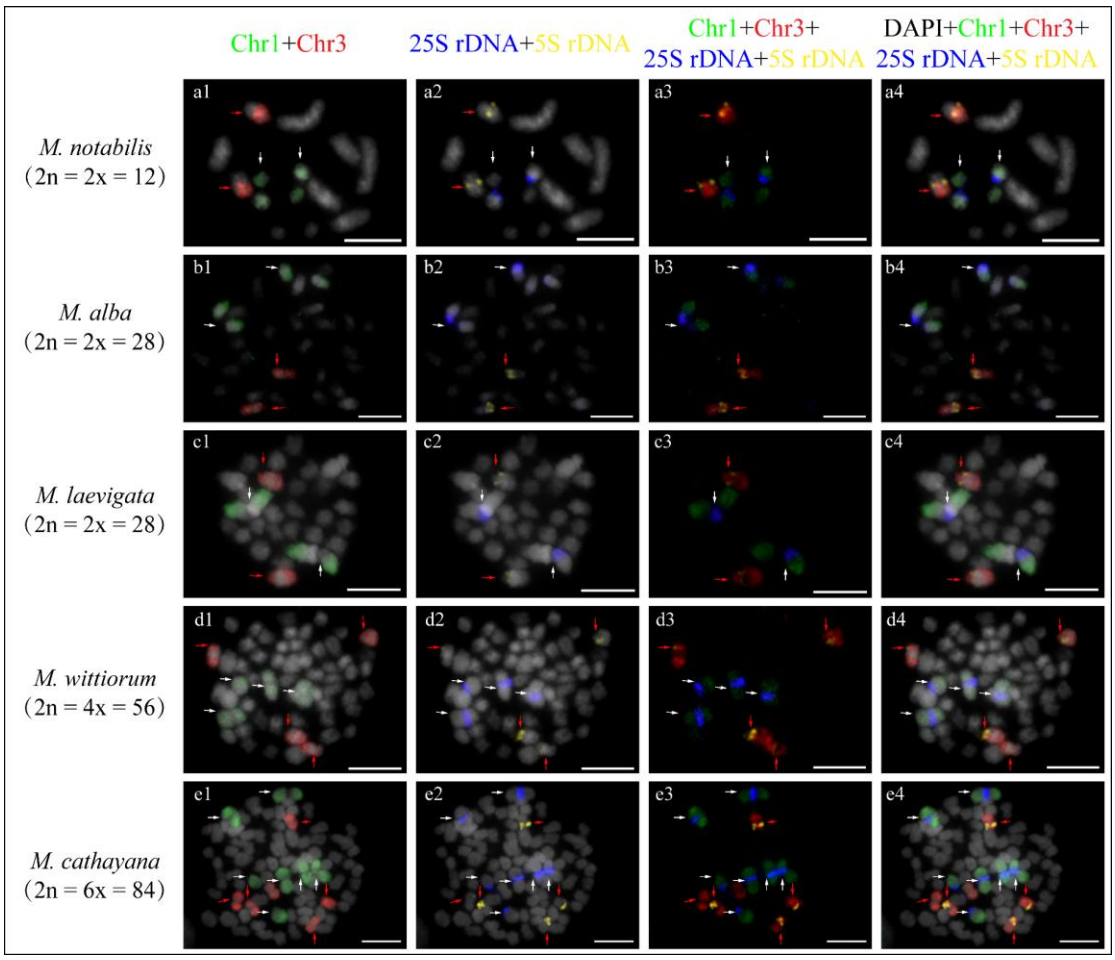

Figure 4. Characterization of 25S and 5S rDNA in five *Morus* species. FISH analysis was performed using the probes from Chr1 painting probe (green), Chr3 painting probe (red), 25S rDNA (blue), and 5S rDNA (yellow). Signals were detected in *M. notabilis* (a1-a4), *M. alba* (b1-b4), *M. laevigata* (c1-c4), *M. wittiorum* (d1-d4), and *M. cathayana* (e1-e4). White and red arrows indicate chromosomes bearing 25S and 5S rDNA loci, respectively. Scale bars represent 5 μm.

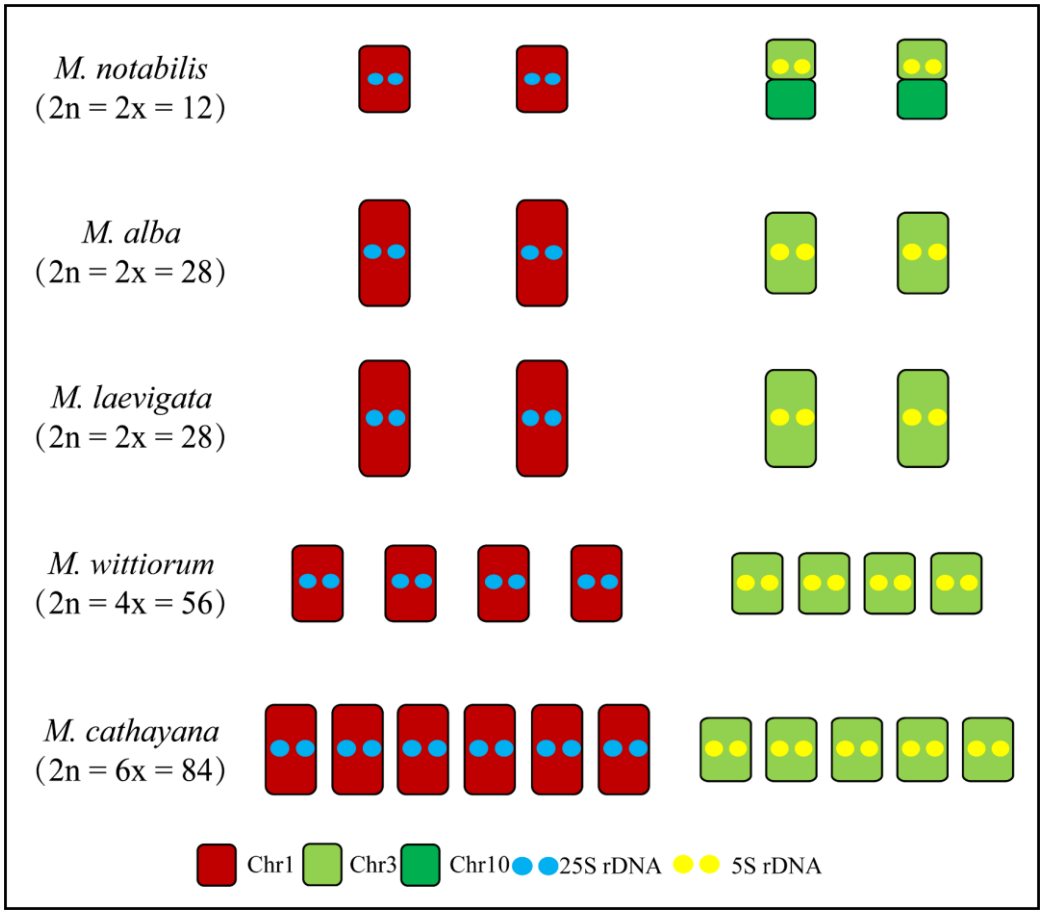

Figure 5. Ideogram illustrating chromosomal locations of 25S and 5S rDNA in *Morus* species. Chr1, Chr3, and Chr10 are identified by their respective painting probes. The positions of 25S rDNA and 5S rDNA FISH signals are indicated.

2.6 Centromere evolution in the genus *Morus* revealed by satellite and telomeric sequences

Based on the *M. alba* genome assembly, a candidate centromeric satellite repeat designated Ma-175 was identified [36,38]. Previous genomic analyses have also demonstrated that *M. notabilis* and *M. mongolica* harbor *Arabidopsis*-type telomeric repeats (TTTAGGG) [44,45]. Accordingly, we performed co-localization assays using Ma-175 and $(TTTAGGG)_4$ to investigate the evolutionary dynamics of centromeric and telomeric regions in the genus *Morus*.

Sequential FISH was performed on *M. laevigata* to determine whether the candidate centromeric sequence Ma-175 could fill the signal gaps on chromosomes 1 and 3. The results revealed a unique and intriguing karyotype: an interspersed arrangement of Ma-175 and $(TTTAGGG)_4$ filled the signal gap

regions in *M. laevigata*, specifically the distal long arm of chromosome 1 and the putative pericentromeric region of chromosome 3 (Figure 6a). By contrast, the remaining chromosomes of *M. laevigata* exhibited a canonical pattern: $(TTTAGGG)_4$ localized at the chromosomal termini and Ma-175 in middle regions (Figure 6a).

To determine whether this unique karyotype of *M. laevigata* is lineage-specific, sequential FISH with Ma-175 and $(TTTAGGG)_4$ was performed on the remaining four *Morus* species: *M. notabilis*, *M. alba*, *M. wittiorum*, and *M. cathayana*. Co-localization analyses on both metaphase chromosomes and interphase nuclei revealed that Ma-175 signals were detected in the putative pericentromeric regions in all species except *M. notabilis*, while $(TTTAGGG)_4$ signals were localized at both chromosomal termini as well as the putative pericentromeric region of chromosome 1 (Figure 6b). Interspecific variation of Ma-175 signals distribution was evident: *M. notabilis* displayed faint and variable numbers of signal bands on each chromosome; *M. alba* exhibited signals on approximately five pairs of chromosomes; *M. wittiorum* showed signals on about half of its chromosomes; and *M. cathayana* displayed signals on all chromosomes (Figure 6b). Except for the detection of numerous interstitial telomeric repeats (ITR) in *M. notabilis*, the $(TTTAGGG)_4$ signal pattern remained largely conserved across species. Notably, only *M. alba* exhibited a spatial organizational pattern analogous to that of *M. laevigata*: Ma-175 and $(TTTAGGG)_4$ were spatially closely associated at the distal end of the long arm of chromosome 1, and this close association was more prominent in interphase nuclei (Figure 6 b3-b4).

Subsequently, we selected six additional *M. laevigata* accessions (designated L-1–L-6) to further validate the lineage specificity of this unique karyotypic feature. Sequential FISH clearly revealed a tight spatial arrangement of Ma-175 and $(TTTAGGG)_4$ on chromosomes 1 and 3 across all examined *M. laevigata* accessions, with this spatial association being even more distinctly resolved in interphase nuclei (Figure 6b). These findings demonstrate that the unique chromosome 3 in *M. laevigata* is strongly species-specific.

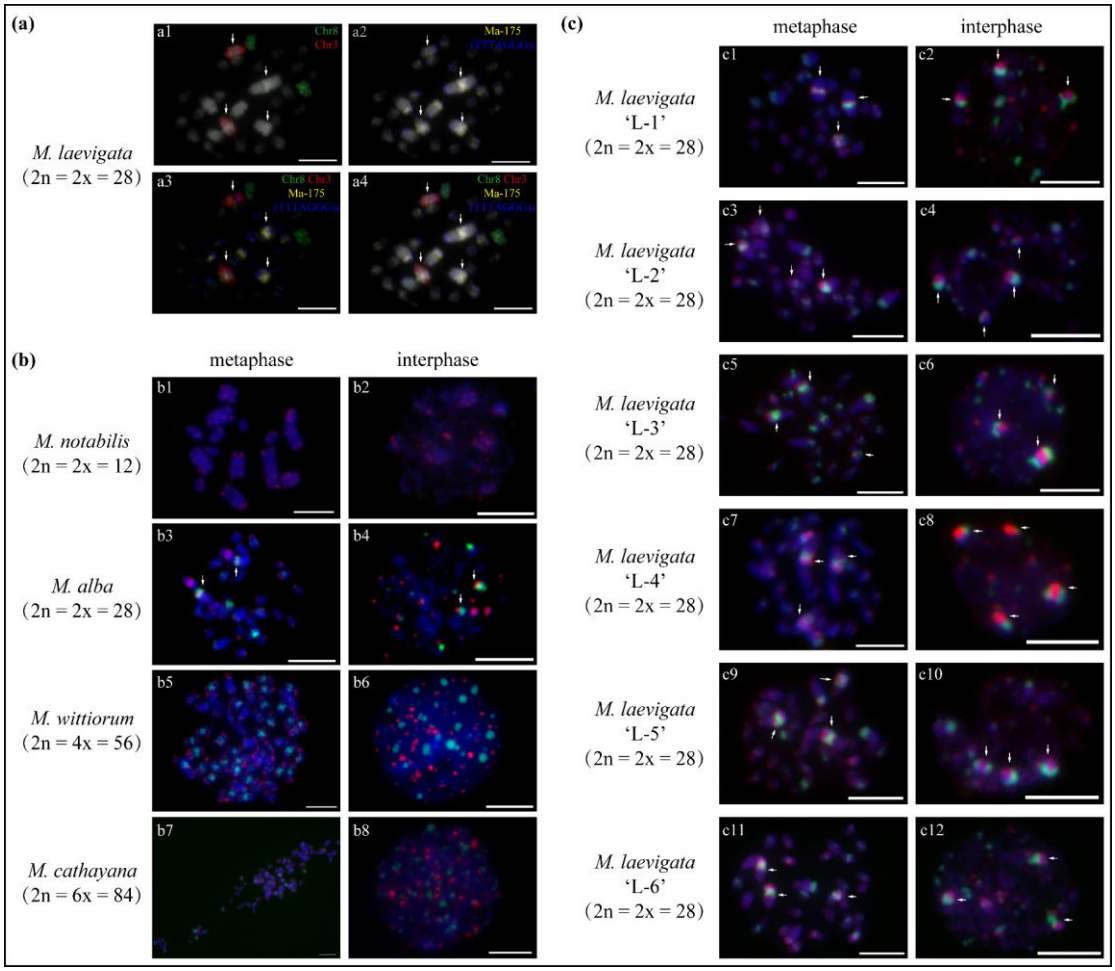

Figure 6. Comparative FISH analysis of candidate centromeric and telomeric sequences in five *Morus* species. (a) Sequential FISH in *M. laevigata* using the Chr8 painting probe (green), Chr3 painting probe (red), $(TTTAGGG)_4$ (blue), and Ma-175 (yellow). (b) Sequential FISH with Ma-175 (green) and $(TTTAGGG)_4$ (red) performed in *M. notabilis* (b1–b2), *M. alba* (b3–b4), *M. wittiorum* (b5–b6), and *M. cathayana* (b7–b8). (c) The same two-round FISH applied to six additional *M. laevigata* accessions ('L-1' to 'L-6'), corresponding to panels c1–c2, c3–c4, c5–c6, c7–c8, c9–c10, and c11–c12, respectively. Panels labeled "metaphase" and "interphase" show mitotic metaphase chromosomes and interphase nuclei, respectively. White arrows indicate chromosomal regions where Ma-175 and $(TTTAGGG)_4$ exhibit tight spatial association. Scale bars represent 5 μm.

2.7 Comparative analysis of chromosome 1 length (orthologous to Mn-Chr5) across *Morus* species

Chromosome 1 of *Morus* species (x=14) is characterized by the longest chromosome length, highly

abundant repetitive sequences, and the presence of chromosomal fusion-fission cycles [34,37,41]. Notably, Mn-Chr5, which shares high homology with chromosome 1 of *Morus* species (x=14), displays the most pronounced differences in both chromosome length and the repetitive sequence distribution.

To further characterize these differences, we measured the total chromosome length and the painting-covered length for chromosome 1 (Mn-Chr5) in five *Morus* species (Supplementary Table 2 and Supplementary Figure 3 a-b). The length variation of unpainted chromosomal regions was subsequently analyzed at both intraspecific and interspecific levels (Supplementary Figure 3c and Supplementary Figure 4). Our results revealed pronounced interspecific differences in total chromosome length: *M. notabilis* exhibited the shortest chromosome, whereas *M. laevigata* possessed the longest (Supplementary Figure 3a). The painted lengths followed a similar trend but with a markedly reduced magnitude of variation (Supplementary Figure 3b). Lengths of unpainted regions also displayed substantial interspecific variation (Supplementary Figure 3c). Notably, *M. notabilis* and *M. wittiorum* exhibited highly comparable chromosome lengths regardless of the measurement metric applied.

2.8 Dynamics of chromosome numbers after γ-WGD in Moraceae

M. notabilis and *B. papyrifera* are among the few species in Rosales that have experienced only the γ-WGD event [29,30]. To date, a lineage specific WGD following the divergence from *Morus* has been reported in *Artocarpus* [31], and widespread polyploids have been observed in the genera *Morus*, *Artocarpus*, and *Ficus* [34,35,46-48]. Building on these observations, we hypothesize that the majority of diploid Moraceae species have experienced only the γ-WGD, without retaining any other genome duplications over the past approximately 100 million years.

We conducted *Ks* analysis on six Moraceae species: *M. notabilis*, *M. alba*, *M. multicaulis*, *M. atropurpurea*, *F. carica*, and *F. hirta* (Supplementary Table 3). Peaks with lower *Ks* values are likely attributable to factors such as expansion of tandemly duplicated gene families [49,50]. The resulting *Ks* values were plotted together with *V. vinifera* [51], which is known to have experienced only the γ-WGD, to generate *Ks* curves (Supplementary Figure 5). These *Ks* curves revealed that all four species have experienced only the γ-WGD (Supplementary Figure 5), a conclusion supported by previous studies [29,30].

Genomic synteny analysis was further employed to investigate the dynamics of basic chromosome numbers after γ-WGD in Moraceae. Comparative genomic analyses were conducted using the *M. alba* genome as reference against ten additional Moraceae genomes. Synteny analysis revealed extensive and complex chromosomal rearrangements within Moraceae (Supplementary Figures 6-7). *Artocarpus heterophyllus* (2n=2x=56) displayed a 2:1 syntenic correspondence with *M. alba*, where two consecutive chromosomes of *A. heterophyllus* aligned to a single chromosome of *M. alba* (Supplementary Figures 6h-7h). Three *Broussonetia* (2n=2x=26) species shared a conserved chromosomal rearrangement: chromosomes 9 and 13 of *M. alba* collinearly corresponded to chromosome 1 of *Broussonetia* (Figure 7 a-b and Supplementary Figures 6-7 (e-f)). The remaining six species each possessed a single intact chromosome syntenic to both chromosomes 10 and 13 of *M. alba* (Figure 7 and Supplementary Figures 6-7). *B. papyrifera* was used to validate the chromosomal rearrangement involving Chr9 and Chr13, while the rearrangement of Chr10 and Chr13 was verified in *F. carica*. Cross-species oligo-painting clearly revealed the rearrangement of Chr9 and Chr13 in *B. papyrifera* and Chr10 and Chr13 in *F. carica*, respectively (Figure 7e). In addition, unique chromosomal rearrangements were observed in *F. microcarpa* and *F. hispida*: two *Ficus* chromosomes correspond to chromosome 1 of *M. alba*, and chromosome 3 of *F. microcarpa* corresponds to two *M. alba* chromosomes (Supplementary Figures 6-7 (a-b)).

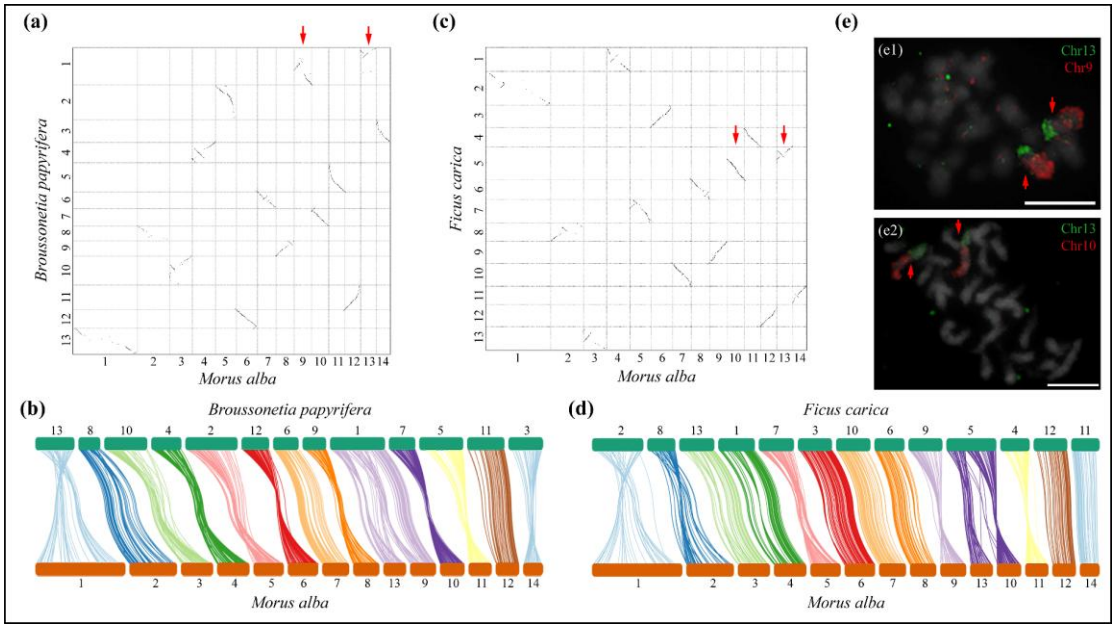

Figure 7. Chromosome-scale synteny comparisons among *M. alba* and two other Moraceae species

(*B. papyrifera* and *F. carica*). (a) Dotplot showing interspecific synteny between *M. alba* (rows) and *B. papyrifera* (columns). (b) Syntenic blocks between *M. alba* and *B. papyrifera*. (c) Dotplot showing interspecific synteny between *M. alba* (rows) and *F. carica* (columns). (d) Syntenic blocks between *M. alba* and *F. carica*. (e) Cytological validation of the syntenic blocks. (e1) FISH analysis using the Chr13 painting probe (green) and Chr9 painting probe (red) in *B. papyrifera*. (e2) FISH analysis using the Chr13 painting probe (green) and Chr10 painting probe (red) in *F. carica*. Red arrows indicate interchromosomal rearrangements. Scale bars represent 5 μm.

2.9 Reconstruction of the ancestral Moraceae karyotype and descending dysploidy in Moraceae

The directionality of chromosomal rearrangements can be inferred from the chromosomal structure of outgroup taxa [52]. Therefore, we reconstructed the ancestral karyotype using WGDI. With *Cannabis sativa* as the outgroup and the genomes of *M. alba*, *M. notabilis*, *F. carica*, *F. hispida*, *F. microcarpa*, and *B. papyrifera*, we identified shared chromosome-like synteny blocks. On this basis, we reconstructed the ancestral Moraceae karyotype (AMK), comprising 14 ancestral chromosomes. The ancestral core eudicot karyotype (ACEK) were mapped onto *C. sativa* and AMK to determine the evolutionary polarity of Moraceae (Supplementary Figures 8-9).

We next closely examined the association between chromosome number variation and chromosomal rearrangement events across the 11 Moraceae species analyzed (Figure 8). *A. nanchuanensis* retained AMK, and it underwent no interchromosomal rearrangements but experienced one lineage-specific WGD (Supplementary Figure 10). In contrast, *M. alba* and *M. atropurpurea* have retained nearly the complete AMK and thus represent the genomic state closest to the ancestral karyotype (Supplementary Figures 11-12). The remaining two *Morus* species analyzed (*M. notabilis* and *M. yunnanensis*) were formed by eight end-to-end joining (EEJ) events that reduced the basic chromosome numbers to six (Supplementary Figures 13-14). In *Broussonetia*, a single EEJ event between AMK1 and AMK10, together with one inversion (INV), gave rise to chromosome 1 of the *B. papyrifera* (Supplementary Figure 15). In *A. toxicaria* analyzed, a single EEJ event resulted in a chromosome number reduced to 13 (Supplementary Figure 16). The genus *Ficus* exhibited a complex chromosomal evolutionary trajectory.

A single EEJ event between AMK7 and AMK10 gave rise to one chromosome in *F. carica* and *F. hirta* (Supplementary Figures 17-18). A subsequent chromosomal fission (Cfis) event restored the chromosome number of *F. hispida* to 14 (Supplementary Figure 19). An EEJ event involving chromosomes 3 and 7 of *F. hispida* ultimately generated *F. microcarpa*, which possesses a complex karyotype comprising 13 chromosomes (Supplementary Figure 20).

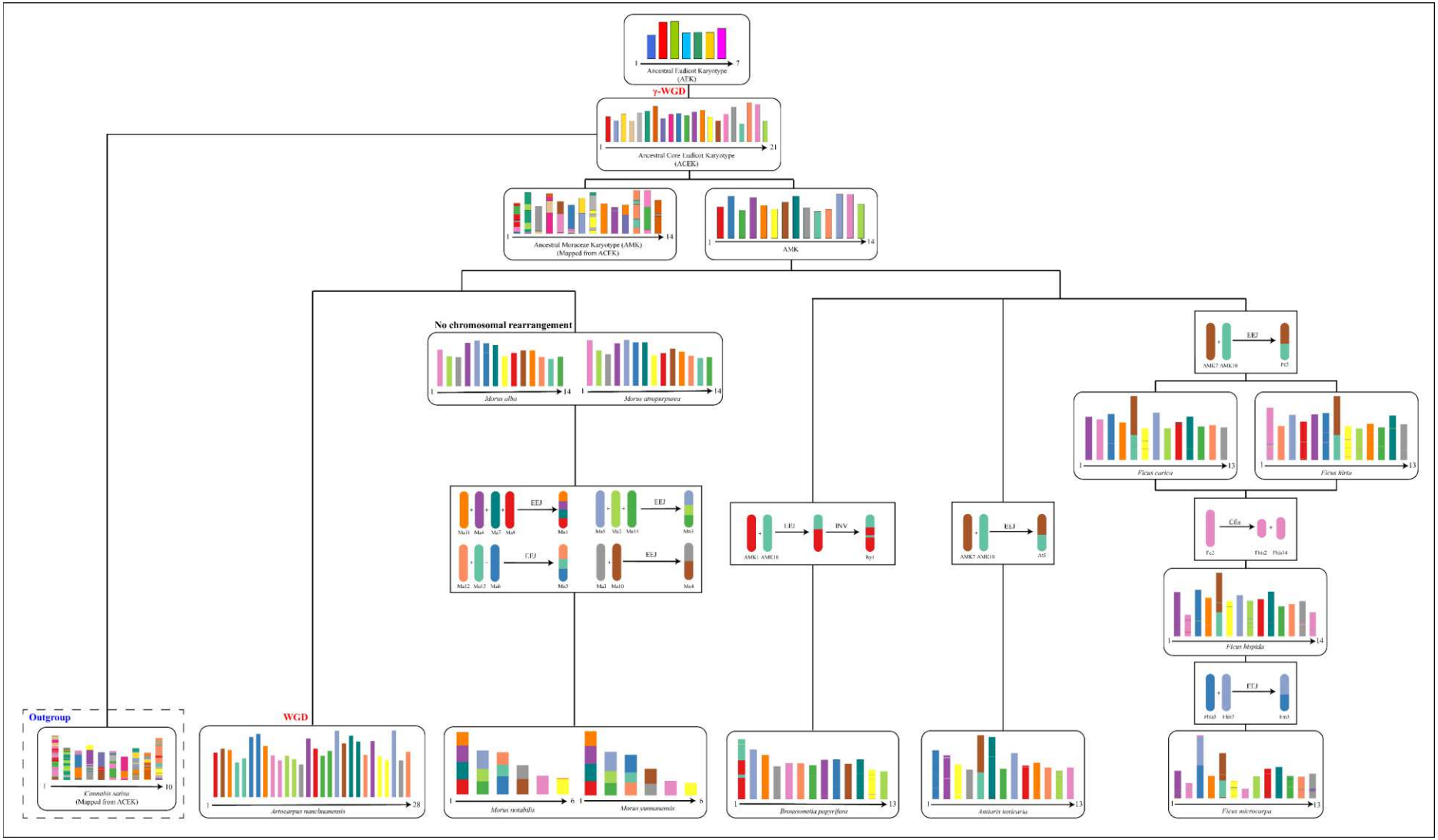
Ancestral Eudicot Karyotype (AEK)
γ-WGD
Ancestral Core Eudicot Karyotype (ACEK)
Ancestral Moraceae Karyotype (AMK) (Mapped from ACEK)
AMK
No chromosomal rearrangement
Morus alba
Morus atropurpurea
EEJ
INV
Outgroup
Cannabis sativa (Mapped from ACEK)
WGD
Artocarpus nanchuanensis
Morus notabilis
Morus yunnanensis
Broussonetia papyrifera
Antiaris toxicaria
Ficus carica
Ficus hirta
Ficus hispida
Ficus microcarpa

Figure 8. Ideograms based on published genome assemblies and reconstruction of the origins of five genera within the Moraceae family using WGDI. *Cannabis sativa* was used as the outgroup. Schematic of phylogenetic relationships based on the phylogenetic analyses by Yang et al. [28]. AEK: ancestral eudicot karyotype; ACEK: ancestral core eudicot karyotype; AMK: ancestral Moraceae karyotype. EEJ: end-to-end joining; INV: inversion; Cfis: chromosomal fission. Ma followed by a number denotes the corresponding chromosome of *M. alba*; for example, Ma2 denotes chromosome 2 of *M. alba*. This is also the case for the remaining Mn, Bp, At, Fc, Fhis, and Fm.

2.10 Gene density variation following chromosomal fusion

To further investigate the impact of chromosome fusion on *Morus*, we compared gene density between the pre-fusion (*M. alba*) and post-fusion (*M. notabilis*) genomes (Supplementary Figure 21). Overall, *M. notabilis* gained more genes following chromosome fusion. In *M. notabilis*, Mn-Chr 1–4 generated by end-to-end fusion events, together with Mn-Chr 5-6, each gained hundreds of genes. Gene density ranged from 18.393 to 54.830 in *M. alba* and from 56.150 to 129.602 in *M. notabilis* (Supplementary Tables 4-5). Notably, Mn-Chr5 and Mn-Chr6, which did not undergo rearrangement, also exhibited higher gene density; in particular, the gene density of Mn-Chr5 was more than threefold that of chromosome 1 in *M. alba*.

3 Discussion

3.1 Lineage-specific WGD shaped polyploidy in Moraceae family

Polyploidization is a ubiquitous phenomenon across almost extant plant species, playing a critical role in shaping genome architecture, driving species diversification, and facilitating crop domestication [53-55]. Recent advances in high-throughput sequencing have greatly facilitated the investigation of plant polyploidization histories, with well-characterized WGD events documented in numerous genera including *Belamcanda*, *Gleditsia*, *Houttuynia*, and *Coptis* [56-60]. WGD events have been also frequently reported in Moraceae. Previous genomic studies have consistently shown that species including *F. microcarpa*, *F. hispida*, *F. altissima*, *F. hirta*, *M. notabilis*, and *B. papyrifera* have retained only the ancestral γ-WGD shared by all eudicots [29,30,33,61]. This pattern was further validated by our *Ks* analysis, which demonstrated that most diploid Moraceae species have undergone only the γ-WGD.

However, exceptions to this pattern exist. Our results reveal a lineage-specific WGD event in *Artocarpus* that doubled the basic chromosome number to 28. *Artocarpus* chromosomes exhibit a clear 2:1 syntenic correspondence relative to Morus, a pattern further supported by comparative genomic analyses [31]. A comparable evolutionary signature was detected in *M. wittiorum* and *M. cathayana*, where oligo-painting revealed homologous copy numbers consistent with their ploidy levels. These observations suggest that the speciation of *M. wittiorum* and *M. cathayana* was also driven by an independent WGD event analogous to that in *Artocarpus*. In addition, widespread natural triploids have been documented in Moraceae [34,35,46-48]. Combined with cytological evidence for the occurrence of 2n gametes in *Morus*, these findings indicate that sexual polyploidization is a significant WGD mechanism in Moraceae— an evolutionary pattern observed in *Brassica*, *Solanum*, and *Turnera* [40,62-66].

Diploidization in plants can be broadly categorized into cytological diploidization and functional diploidization (gene fractionation) [67,68]. These two processes are relatively independent and collectively driving extensive lineage diversification during post-polyploid diploidization [69,70]. In this study, using conserved oligo probes derived from the diploid *M. alba*, we detected homologous copy numbers in the polyploid species *M. wittiorum* (tetraploid) and *M. cathayana* (hexaploid) that matched their ploidy levels. The lack of differential fluorescence intensity among these copies implies that subgenomic sequence divergence in these two species is relatively limited. The production of abundant euploid seeds by *M. wittiorum* attests to its regular meiosis [40]. Together, these observations suggest that *M. wittiorum* is neopolyploids: although it exhibit meiotic stability, it may be at an initial stage of post-polyploid diploidization.

3.2 Chromosomal fusion is the primary driver of genomic evolution in Moraceae

Chromosomal rearrangements are a core driver of plant speciation and evolution, promoting species formation and thereby driving lineage diversification [71-73]. A key mechanism in this process is chromosome fusion, which reduces the chromosome number [74-76]. Complex chromosomal rearrangements ultimately generated the remarkable species diversity observed in extant Moraceae [77]. Our results demonstrate that Moraceae species tend toward a reduction in chromosome number during

evolution, with differential chromosomal rearrangements directly promoting lineage diversification within the family. The reduction in basic chromosome numbers also possibly provided a favorable chromosomal architecture for stable inheritance in Moraceae. Specifically, *Antiaris*, *Broussonetia*, and *Ficus* each share unique chromosome fusion events that account for their reduced chromosome numbers. *F. microcarpa* and *F. hispida* share a common Cfis event, in which two chromosomes correspond to chromosome 1 of *Morus* (x=14). Subsequently, *F. microcarpa* underwent a species-specific chromosomal fusion that differentiated its karyotype from that of *F. hispida*. Based on these findings, we propose that chromosomal fusion serves as a core driver of chromosomal evolution in Moraceae.

M. alba and *M. atropurpurea* are the species closest to the AMK among all Moraceae species analyzed, having experienced virtually no chromosomal rearrangements. This indicates that oligo probes designed from M. alba can be practically used as probes for the AMK, which enables efficient and convenient analysis of karyotype evolution in Moraceae, particularly in species lacking genome assemblies. Notably, the congeneric species *M. notabilis* and *M. yunnanensis* are characterized by eight EEJ events in their chromosomal structure, which shaped a unique karyotype. Cytological evidence indicates that *M. notabilis* harbors ITR loci on every chromosomes, which are presumed to reflect a "pioneer state" in Moraceae evolution. This fusion-mediated pattern of chromosomal evolution is strikingly consistent with that observed in *Luzula,* and the polycentric characteristics of *M.* notabilis also resemble to this model [44,78]. Chromosome fusion eliminates original telomeric sequences, thereby relieving the repressive effect of adjacent genes and altering the relative positions of genes flanking the fusion junction [79,80]. Moreover, following chromosomal fusion, each chromosome of M. notabilis gained more genes and exhibited higher gene density. This indirectly suggests that chromosomal fusion endowed M. notabilis with a richer gene reservoir, providing it with a potential genetic advantage. Therefore, we propose that chromosome fusion holds evolutionary significance in Moraceae and may have contributed to enhanced adaptability through multiple functional dimensions.

3.3 Chromosomal rearrangements drive lineage-specific diversification in lineages with only γ-WGD

γ-WGD served as an important genomic basis for the diversification burst of core eudicots, generating a highly repetitive genomic architecture (x = 21) in the ancestor of core eudicots [81,82]. Some lineages (such as *Fabaceae* and *Brassicaceae*) further increased genomic dosage and expanded the gene repertoire by superimposing additional lineage-specific WGDs (e.g., α- and β-WGD) [83,84]. In contrast, "γ-only" lineages exhibit an alternative evolutionary pathway: without increasing genomic dosage, they can still evolve extensive morphological and ecological adaptations through the differential retention/loss, subfunctionalization/neofunctionalization of γ-derived duplicated genes, and structural rearrangements [85,86].

Furthermore, γ-only species exhibit extreme variation in chromosome number, ranging from the ACEK (x=21) and the near-ancestral state in *V. vinifera* (x=19) to the highly rearranged *M. notabilis* (x=6) and *Paeonia ludlowii* (x=5) [87,88]. In the absence of "interference" from additional WGDs, such structural variations directly reveal how the genetic redundancy generated by γ-WGD has been resolved and remodeled over extended evolutionary time. Such genomic remodeling can follow diverse evolutionary trajectories even within a single family. For instance, in Vitaceae, most species retain a state similar to the ancestral Vitaceae karyotype, while *Cissus rotundifolia* has undergone extensive chromosomal rearrangements [88]. A similar pattern was observed in Moraceae: *B. papyrifera* and *A. toxicaria* underwent only a single EEJ event, whereas *M. notabilis* and *M. yunnanensis* experienced eight EEJ events. Collectively, these observations suggest that the genomic evolution of γ-only lineages is not a passive process, but rather a highly lineage-specific and dynamic trajectory. The absence of additional WGDs does not equate to karyotypic stasis; instead, chromosomal rearrangements (e.g., EEJ and Cfis) and localized gene amplification serve as core drivers in reshaping ancestral γ-derived architectures.

3.4 Karyotypic conservatism masks complex chromosomal evolution and repetitive sequence dynamics that drive speciation in *Morus*

The high-resolution oligo-painting technique enables the identification of most chromosomal regions across species and has been widely applied in genera such as *Aegilops*, *Cucumis*, and *Glycyrrhiza* [89-93]. In this study, we employed oligo-painting to detect conserved chromosomal regions among five *Morus* species. With the exception of *M. notabilis*, all examined *Morus* species exhibited stable karyotypes.

However, beneath this seemingly conserved karyotype lies complex karyotypic evolution and substantial genetic diversity.

The co-localization of centromeric and telomeric sequences is a phenomenon frequently observed in nature, likely attributable to end-to-end chromosome fusions and nested chromosome fusions [94-96]. In the present, study, cross-arrangement or co-localization of candidate centromeric sequences and telomeric sequences was detected on chromosome 1 (Mn-Chr5) across all *Morus* species. We infer that this may have resulted from telomeric remnants retained during the ACEK-to-AMK transition, and these remnants may also have contributed to the differentiation of the genus *Morus*. Notably, a similar co-localization pattern was also detected on chromosome 3 in all accessions of *M. laevigata*, suggesting that this structural variation is lineage-specific of *M. laevigata*. We further constructed distribution maps of repetitive sequences on chromosomes 1 and 3 of *M. alba* and *M. laevigata* (Supplementary Fig 22a). The resulting maps revealed marked structural divergence between the two species, despite their identical ploidy and superficially similar karyotypes (Supplementary Fig 22a). Building on these observations, we reconstructed the putative evolutionary pathway underlying the lineage-specific structural rearrangement in *M. laevigata* (Supplementary Fig 22b). We therefore consider that karyotypic evolution is a primary driver underlying speciation in *Morus*.

3.5 Elimination of genomic redundancy confers evolutionary advantages in *M. notabilis*

Chromosome 1 (Mn-Chr5) displays the most remarkable genomic features in *Morus*. Among diploid species, it harbors the highest abundance of repetitive sequences. In polyploids, however, these sequences are greatly reduced on chromosome 1 and dispersing across other chromosomes. These genomic characteristics were consistently corroborated by the localization of candidate centromeric sequences, telomeric sequences, and genomic probes [34].

Marked interspecific length variation is detected on *Morus* chromosome 1 (Mn-Chr5). As reported in *Cucurbita* [43], repetitive sequences appear to drive chromosome length variation in *Morus*. Mn-Chr5 has lost most of its repetitive sequences and consequently exhibits the shortest length, likely reflecting the

elimination of redundant genomic components during chromosomal fusion while preserving functional integrity. The loss of repetitive sequences was accompanied by alterations in the relative positions of genes; meanwhile, Mn-Chr5 exhibited a markedly higher gene number and gene density than chromosome 1 of *M. alba*. The position effects arising from the combination of these two factors may have had beneficial effects on *M. notabilis*. We hypothesize that this reduction in genomic redundancy may have facilitated speciation in *M. notabilis*. This redundancy-depleted chromosome 5, shaped by natural selection, likely confers potential evolutionary advantages to *M. notabilis* as a newly diverged lineage.

4 Materials and methods

4.1 Plant materials and chromosome preparation

In this study, seven materials were selected for oligo-painting analysis. These materials comprised five mulberry accessions (*M. notabilis*, *M. alba*, *M. laevigata*, *M. wittiorum*, and *M. cathayana*), one paper mulberry accession (*Broussonetia papyrifera*), and one fig accession (*Ficus carica*). Six additional *M. laevigata* accessions were utilized for the detection of the Ma-175 and telomeric probes. Mitotic metaphase chromosome preparation was performed following previously published protocols [37]. All plant materials were preserved through grafting or seeding in the Mulberry Germplasm Nursery at Southwest University, Chongqing, China. Detailed information regarding the accessions, including those used for genomic DNA extraction and chromosome preparation, is presented in Supplementary Table 6.

4.2 Development of chromosome-specific oligo-painting probes

The chromosome-level reference genome of *M. alba* was downloaded from the Genome Warehouse [97] (PRJNA597121) of the National Genomics Data Center [38,98]. Single-copy 45 nucleotide (nt) oligonucleotides (oligos) were generated using Chorus2 [39].

To identify *Morus*-conserved oligos, the raw oligo sequences were aligned to the reference genome of *M. notabilis*, and only successfully mapped sequences were retained [36]. Subsequently, the selected oligo sequences were further filtered for potential repetitive sequences in the short-read sequencing data using the scripts ChorusNGSfilter.py and ChorusNGSselect.py [36,38,39]. A total of 459,405 conserved oligos were

obtained after filtering. Oligo density was calculated in 500-kb sliding windows, and the distribution of these oligos was visualized on chromosome ideograms.

4.3 Synthesis of chromosome-specific probes

Chromosome-specific primers were added to both ends of the specific oligos for individual chromosomes. Chromosome-specific oligos were synthesized by Synbio Technologies (Suzhou, China; http://www.synbio-tech.com.cn) into a pooled library. Primers labeled with FAM or TAMRA fluorophores at their 5′ ends were synthesized by Zixi Biotechnology (Beijing, China; http:// https://www.tsingke.com.cn/). Detailed information on all primers is documented in Supplementary Table 7.

Pooled chromosome-specific oligo probes were prepared using a two-step PCR amplification system [99]. The 50 μL PCR reaction mixture contained 0.14 ng of oligo library DNA, 2 μL of 100 μM fluorescence-labeled forward primer, 2 μL of 100 μM fluorescence-labeled reverse primer, 25 μL of KAPA HiFi HotStart ReadyMix (Roche, CHE), and double-distilled water (ddH_2O) to a final volume of 50 μL. The PCR amplification program was adapted from the multiplex PCR protocol for cucumber [99], and the program was set as follows: pre-denaturation at 95℃ for 5 min; 15 cycles of 95℃ for 15 s, 68℃ for 15 s, and 72℃ for 15 s; 25 cycles of 95℃ for 15 s, 60℃ for 15 s, and 72℃ for 15 s; and a final extension at 72℃ for 10 min. The PCR products were purified using the GeneJET PCR Purification Kit (Thermo Fisher Scientific, USA) and eluted with 20 μL of ddH_2O to yield the labeled oligo probes.

4.4 Synthesis and labeling of candidate centromere, rDNAs, and telomere probes

According to previously published studies, 175-bp satellite sequences were screened as candidate centromeric sequences in the *M. alba* genome using Tandem Repeats Finder [36,100]. The Ma-175 sequence was amplified with the Ma-175 F/R primer pair using *M. alba* genome as the template. Amplification of the 25S rDNA and 5S rDNA sequences was carried out following previously reported protocols [41]. Detailed information on all the primers mentioned above is listed in Supplementary Table 7.

PCR products were purified using purification kits (Omega, USA), and the probes were labeled by nick

translation: Ma-175 and 25S rDNA probes were labeled with ChromaTide Alexa Fluor 488-5-dUTP (Thermo Fisher Scientific [Invitrogen], Massachusetts, USA), while the 5S rDNA probe was labeled with Texas-Red-5-dCTP (PerkinElmer, Massachusetts, USA). The *Arabidopsis*-type telomeric probe $(TTTAGGG)_4$ labeled with TAMRA fluorophore at the 5′ end was synthesized by Zixi Biotechnology.

4.5 Oligo-painting and fluorescence *in situ* hybridization

Oligo-painting experiments were performed according to previously published protocols [99]. The hybridization mixture was composed of 10 μL formamide, 2 μL of 20×SSC, 4 μL of 50% dextran sulfate, 2 μL of TAMRA-labeled and 2 μL of FAM-labeled oligo probes. The hybridization mixture was denatured at 85℃ for 10 min and immediately placed on ice for at least 5 min. Chromosome slides were denatured in 70% formamide (dissolved in 2×SSC) at 80℃ for 3 min, rapidly dehydrated in a series of pre-chilled ethanol solutions (70%, 90%, 100%) at -20℃ for 3 min each, and dried quickly at 42℃ for 20 s. The denatured hybridization mixture was dropped onto the slides, followed by overnight hybridization at 37℃. The slides were washed as follows: 2×SSC for 5 min at room temperature, 2×SSC for 10 min at 42℃, 2×SSC for 5 min at room temperature, 1×PBS for 5 min at room temperature, and 2×SSC for 5 min at room temperature. The slides were counterstained with 4′,6-diamidino-2-phenylindole (DAPI) at 1 ng/μL and sealed with nail polish.

FISH analysis was conducted following our previously established protocol [34]. For ND-FISH, the protocol was modified from Jiang et al. as follows [101]: the hybridization mixture contained 500 ng $(TTTAGGG)_4$ probe, adjusted to a final volume of 10 μL with 2×SSC + 1×TE. After hybridization at 42℃ for 3 h, the slides were washed three times in 2×SSC at 42℃ for 5 min each. The slides were counterstained with DAPI (1 ng/μL) and sealed with nail polish.

For sequential rounds of FISH, coverslips were removed by covering slides with 1×PBS for 5 min. Probes were stripped by incubating slides in 50% formamide (containing 2×SSC) at 42℃ for 10 min twice. After dehydration in an ethanol series (70%, 90%, 100%, 3 min each at room temperature), the slides were stored at 37℃ for the subsequent rounds of FISH.

Images of counterstained slides were captured using an Olympus DP80 CCD camera (Olympus, Japan) attached to an Olympus IX73 fluorescence microscope and processed using Adobe Photoshop 2021 and Adobe Illustrator 2021 (Adobe, USA). Chromosome lengths were measured using ImageJ (https://imagej.net/ij/) in at least five mitotic metaphase cells with no obvious morphological differences. Statistical analysis and visualization were performed using GraphPad Prism (https://www.graphpad.com/features).

4.6 Synonymous substitution rate analysis

For WGD analysis of Moraceae species, synonymous substitution rate (*Ks*) values were calculated using WGDI for *M. notabilis*, *M. alba*, *M. multicaulis*, *M. atropurpurea*, *F. carica*, and *F. hirta* [33,44,102-105]. Gaussian mixture models were fitted using the mclust package in R [106]. The *Ks* peak plot was subsequently generated alongside *Vitis vinifera*, which underwent only the γ-WGD event [51].

4.7 Genomic synteny analysis

Synteny between the model mulberry species *M. alba* and the other ten Moraceae species (*F. microcarpa*, *F. hispida*, *F. hirta*, *F. benjamina*, *F. carica*, *B. papyrifera*, *B. kaempferi*, *B. monoica*, *A. heterophyllus*, and *Antiaris toxicaria*) was analyzed using Chromeister, and the results were visualized as comparative dotplots [31,38,107-111]. Additionally, whole-genome synteny alignments were aligned with MUMmer4 (https://github.com/mummer4/mummer) and visualized using pyGenomeViz (https://github.com/moshi4/pyGenomeViz/) [112]. Detailed information on all the genomes mentioned above is listed in Supplementary Table 8.

4.8 Reconstruction of the ancestral Moraceae karyotype

We applied WGDI to identify protochromosomes and reconstruct the ancestral Moraceae genome according to previous studies [52,104,113]. Briefly, with *Cannabis sativa* as the outgroup, we identified conserved blocks within the genomes of *M. alba*, *M. notabilis*, *F. carica*, *F. hispida*, *F. microcarpa*, and *B. papyrifera* using DIAMOND, and reconstructed the ancestral Moraceae genome [33,44,102,103,114]. The data for the ancestral eudicot karyotype (AEK) and ancestral core eudicot karyotype (ACEK) were obtained from https://github.com/SunPengChuan. The WGDI toolkit with the "-km" parameter was used

to map the fourteen proto-chromosomes of the inferred AMK onto the chromosomes of the 11 sampled genomes [33,44,77,102-105,110,111,115].

4.9 Gene density calculation

Gene density of *M. alba* and *M. notabilis* was calculated using a sliding window strategy [44,103]. Briefly, the assembled chromosome sequences were divided into non-overlapping 0.5-Mb windows. The number of annotated genes located within each window was counted, and gene density was defined as the number of genes per 0.5 megabase (genes/0.5 Mb). The resulting gene density values were visualized in R.

5 Electronic supplementary information

All data generated or analyzed during this study are included in this published article (and its Supplementary Files).

6 CRediT authorship contribution statement

Qiming Zhou: Data curation, Methodology, Visualization, Writing – original draft, Writing – review & editing. **Ziang Li**: Methodology, Visualization, Writing – review & editing. **Jiacheng Li**: Visualization, Data curation. **Yaning Liu**: Visualization. **Jiali Qiu**: Visualization. **Jianglian Yuan**: Resources. **Zhengang Li**: Resources. **Song Chen**: Resources. **Yahui Xuan**: Methodology, Data curation, Visualization . **Ningjia He**: Conceptualization, Writing – review & editing, Funding acquisition.

7 Acknowledgements

We are grateful to Professor Qunfeng Lou from Nanjing Agricultural University for her assistance in optimizing the oligo-painting protocol. We acknowledge the support from the Naban River Watershed National Nature Reserve Administration, Zhenyuan Management and Protection Bureau of Ailao Mountain National Nature Reserve Administration in Yunnan Province, and Baoshan Agricultural Science Research Institute (Baoshan Agricultural Technology Extension Center) for their assistance in the sample collection permissions.

This work was supported by the National Key Research and Development Program of China (Grant No. 2024YFD2201302), the Science and Technology Pilot Project-Key Research and Development Project

(Grant No. SWU-XDZD22008), the Fundamental Research Funds for the Central Universities (SWU-KQ24048), Chongqing Mulberry Germplasm Repository at Beibei (Grant No. ZWZZ20240002), and Zhonghuai Xiang Academician Workstation Project, Yunnan province, China (Grant No. 202305AF150166).

8 Ethics approval and consent to participate

All experimental methods, including the collection of plant materials, complied with relevant institutional, national, and international guidelines and legislation. The voucher specimens of all plants are deposited at the Mulberry Germplasm Nursery at Southwest University, Chongqing, China.

9 Conflict of interest

On behalf of all authors, the corresponding author states that there is no conflict of interest.

10 Data Availability

The plant materials reported in the manuscript are included in Supplementary Table 6 and are freely available to all the readers upon reasonable request.

11 References

1. Van De Peer, Y., Mizrachi, E., and Marchal, K. (2017). The evolutionary significance of polyploidy. Nature Reviews Genetics *18*, 411-424. 10.1038/nrg.2017.26.
2. Salman-Minkov, A., Sabath, N., and Mayrose, I. (2016). Whole-genome duplication as a key factor in crop domestication. Nature Plants *2*, 16115, 16115. 10.1038/nplants.2016.115.
3. Mable, B.K., Alexandrou, M.A., and Taylor, M.I. (2011). Genome duplication in amphibians and fish: an extended synthesis. Journal of Zoology *284*, 151-182. 10.1111/j.1469-7998.2011.00829.x.
4. Otto, S.P., and Whitton, J. (2000). POLYPLOID INCIDENCE AND EVOLUTION. Annual Review of Genetics *34*, 401-437. https://doi.org/10.1146/annurev.genet.34.1.401.
5. Healey, A.L., Garsmeur, O., Lovell, J.T., Shengquiang, S., Sreedasyam, A., Jenkins, J., Plott, C.B., Piperidis, N., Pompidor, N., Llaca, V., et al. (2024). The complex polyploid genome architecture of sugarcane. Nature *628*, 804-810. 10.1038/s41586-024-07231-4.
6. Walkowiak, S., Gao, L.L., Monat, C., Haberer, G., Kassa, M.T., Brinton, J., Ramirez-Gonzalez, R.H., Kolodziej, M.C., Delorean, E., Thambugala, D., et al. (2020). Multiple wheat genomes reveal global variation in modern breeding. Nature *588*, 277-283. 10.1038/s41586-020-2961-x.
7. Wang, J.G., Li, X.F., Wang, Y.B., Lin, J.S., Chen, S., Liu, H.B., Chen, X., Chai, K., Dong, A.Q., Zhao, T.T., et al. (2026). Genetic architecture of sugarcane traits in a polyploid genomics

framework. Nature *654*, 994-1003. 10.1038/s41586-026-10576-7.

8. Yan, H., Han, J.L., Jin, S.K., Han, Z.G., Si, Z.F., Yan, S.Y., Xuan, L.S., Yu, G.R., Guan, X.Y., Fang, L., et al. (2025). Post-polyploidization centromere evolution in cotton. Nature Genetics *57*, 1021–1030. 10.1038/s41588-025-02115-3.

9. Liu, M.Y., Sun, W.J., Li, C.R., Yu, G.L., Li, J.H., Wang, Y.D., and Wang, X. (2021). A multilayered cross-species analysis of GRAS transcription factors uncovered their functional networks in plant adaptation to the environment. Journal of Advanced Research *29*, 191-205. 10.1016/j.jare.2020.10.004.

10. Scarrow, M., Wang, Y.L., and Sun, G.L. (2021). Molecular regulatory mechanisms underlying the adaptability of polyploid plants. Biological Reviews *96*, 394-407. 10.1111/brv.12661.

11. Zhou, K., Liu, B.B., Wang, Y.L., Zhang, X.Q., and Sun, G.L. (2019). Evolutionary mechanism of genome duplication enhancing natural autotetraploid sea barley adaptability to drought stress. Environmental and Experimental Botany *159*, 44-54. 10.1016/j.envexpbot.2018.12.005.

12. Peeters, M.K.R., and van de Peer, Y. (2026). Polyploidy: A macromutational force pushing bioeconomic developments. Proceedings of the National Academy of Sciences *123*, e2522065123, e2522065123. 10.1073/pnas.2522065123.

13. Song, X., Zhang, M., Wang, T.T., Duan, Y.Y., Ren, J., Gao, H., Fan, Y.J., Xia, Q.M., Cao, H.X., Xie, K.D., et al. (2025). Polyploidization leads to salt stress resilience via ethylene signaling in citrus plants. New Phytologist *246*, 176-191. 10.1111/nph.20428.

14. Sun, W.A., Xia, L.J., Deng, J.W., Sun, S.M., Yue, D.D., You, J.Q., Wang, M.J., Jin, S.X., Zhu, L.F., Lindsey, K., et al. (2024). Evolution and subfunctionalization of *CIPK6* homologous genes in regulating cotton drought resistance. Nature Communications *15*, 5733, 5733. 10.1038/s41467-024-50097-3.

15. Jiao, Y.N., Wickett, N.J., Ayyampalayam, S., Chanderbali, A.S., Landherr, L., Ralph, P.E., Tomsho, L.P., Hu, Y., Liang, H.Y., Soltis, P.S., et al. (2011). Ancestral polyploidy in seed plants and angiosperms. Nature *473*, 97-100. 10.1038/nature09916.

16. Comai, L. (2005). The advantages and disadvantages of being polyploid. Nature Reviews Genetics *6*, 836-846. 10.1038/nrg1711.

17. Wendel, J.F., Lisch, D., Hu, G.J., and Mason, A.S. (2018). The long and short of doubling down: polyploidy, epigenetics, and the temporal dynamics of genome fractionation. Current Opinion in Genetics & Development *49*, 1-7. 10.1016/j.gde.2018.01.004.

18. Dodsworth, S., Chase, M.W., and Leitch, A.R. (2016). Is post-polyploidization diploidization the key to the evolutionary success of angiosperms? Botanical Journal of the Linnean Society *180*, 1-5. 10.1111/boj.12357.

19. Liu, B., and Wendel, J.F. (2003). Epigenetic phenomena and the evolution of plant allopolyploids. Molecular Phylogenetics and Evolution *29*, 365-379. 10.1016/s1055-7903(03)00213-6.

20. Qiao, X., Li, Q.H., Yin, H., Qi, K.J., Li, L.T., Wang, R.Z., Zhang, S.L., and Paterson, A.H. (2019). Gene duplication and evolution in recurring polyploidization-diploidization cycles in plants. Genome Biology *20*, 38, 38. 10.1186/s13059-019-1650-2.

21. Griffiths, S., Sharp, R., Foote, T.N., Bertin, I., Wanous, M., Reader, S., Colas, I., and Moore, G. (2006). Molecular characterization of *Ph1* as a major chromosome pairing locus in polyploid wheat. Nature *439*, 749-752. 10.1038/nature04434.

22. Salse, J., Bolot, S., Throude, M., Jouffe, V., Piegu, B., Quraishi, U.M., Calcagno, T., Cooke, R.,

Delseny, M., and Feuillet, C. (2008). Identification and characterization of shared duplications between rice and wheat provide new insight into grass genome evolution. The Plant cell *20*, 11-24. 10.1105/tpc.107.056309.

23. Luo, M.C., Deal, K.R., Akhunov, E.D., Akhunova, A.R., Anderson, O.D., Anderson, J.A., Blake, N., Clegg, M.T., Coleman-Derr, D., Conley, E.J., et al. (2009). Genome comparisons reveal a dominant mechanism of chromosome number reduction in grasses and accelerated genome evolution in Triticeae. Proceedings of the National Academy of Sciences *106*, 15780-15785. 10.1073/pnas.0908195106.
24. Plačková, K., Bureš, P., Lysak, M.A., and Zedek, F. (2024). Centromere drive may propel the evolution of chromosome and genome size in plants. Annals of botany *134*, 1067-1076. 10.1093/aob/mcae149.
25. Wei, F., Coe, E., Nelson, W., Bharti, A.K., Engler, F., Butler, E., Kim, H., Goicoechea, J.L., Chen, M., Lee, S., et al. (2007). Physical and genetic structure of the maize genome reflects its complex evolutionary history. PLoS genetics *3*, e123. 10.1371/journal.pgen.0030123.
26. Vogel, J.P., Garvin, D.F., Mockler, T.C., Schmutz, J., Rokhsar, D., Bevan, M.W., Barry, K., Lucas, S., Harmon-Smith, M., Lail, K., et al. (2010). Genome sequencing and analysis of the model grass *Brachypodium distachyon*. Nature *463*, 763-768. 10.1038/nature08747.
27. Bowers, J.E., and Paterson, A.H. (2021). Chromosome number is key to longevity of polyploid lineages. New Phytologist *231*, 19-28. 10.1111/nph.17361.
28. Yang, C.-X., Liu, S.-Y., Tian, Q., Gu, W., Lu, Q., Guralnick, R.P., Stull, G.W., Kates, H.R., Folk, R.A., Soltis, D.E., et al. (2026). Phylogenomic conflict in Moraceae: Evidence for pervasive introgression and incomplete lineage sorting. Plant Diversity. https://doi.org/10.1016/j.pld.2026.04.003.
29. He, N.J., Zhang, C., Qi, X.W., Zhao, S.C., Tao, Y., Yang, G.J., Lee, T.H., Wang, X.Y., Cai, Q.L., Li, D., et al. (2013). Draft genome sequence of the mulberry tree *Morus notabilis*. Nature Communications *4*, 3445, 2445. 10.1038/ncomms3445.
30. Peng, X.J., Liu, H., Chen, P.L., Tang, F., Hu, Y.M., Wang, F.F., Pi, Z., Zhao, M.L., Chen, N.Z., Chen, H., et al. (2019). A Chromosome-Scale Genome Assembly of Paper Mulberry (*Broussonetia papyrifera*) Provides New Insights into Its Forage and Papermaking Usage. Molecular Plant *12*, 661-677. 10.1016/j.molp.2019.01.021.
31. Lin, X.G., Feng, C., Lin, T., Harris, A.J., Li, Y.Z., and Kang, M. (2022). Jackfruit genome and population genomics provide insights into fruit evolution and domestication history in China. Horticulture Research *9*, uhac173, uhac173. 10.1093/hr/uhac173.
32. Ren, S.X., Gu, X., Chen, Z.X., Liu, Y.X., Zhao, X.Y., Wang, Y.W., Lu, J.K., Cui, J.W., Si, Y.H., Zhang, Y.H., et al. (2025). A chromosome-level genome assembly for *Ficus carica* provides genetic insights into flowerless fig fruit development, psoralen biosynthesis, and drought tolerance. Plant communications *6*, 101470, 101470. 10.1016/j.xplc.2025.101470.
33. Zhang, X.T., Wang, G., Zhang, S.C., Chen, S., Wang, Y.B., Wen, P., Ma, X.K., Shi, Y., Qi, R., Yang, Y., et al. (2020). Genomes of the Banyan Tree and Pollinator Wasp Provide Insights into Fig-Wasp Coevolution. Cell *183*, 875-889. 10.1016/j.cell.2020.09.043.
34. Xuan, Y.H., Wang, S., Li, S.W., Yuan, J.L., Zhou, Q.M., and He, N.J. (2023). Chromosome constitution and genetic relationships of *Morus* spp. revealed by genomic *in situ* hybridization. BMC Plant Biology *23*, 428, 428. 10.1186/s12870-023-04448-9.
35. Falistocco, E. (2016). Recurrent Events of Polyploidy in *Ficus carica* L. (Moraceae).

International Journal of Plant Sciences *177*, 319-325. 10.1086/684275.

36. Xuan, Y.H., Ma, B., Li, D., Tian, Y., Zeng, Q.W., and He, N.J. (2022). Chromosome restructuring and number change during the evolution of *Morus notabilis* and *Morus alba*. Horticulture Research *9*, uhab030, uhab030. 10.1093/hr/uhab030.

37. Zhou, Q.M., Xuan, Y.H., Li, J.C., Qiu, J.L., Yuan, J.L., Fan, C.M., Li, Z.A., Li, S.S., Hu, Z.M., Li, S.W., and He, N.J. (2025). Cytological identification of a genus-wide chromosomal fusion-fission cycles in genus *Morus*. Genetic Resources and Crop Evolution *72*, 6435-6445. 10.1007/s10722-024-02312-9.

38. Jiao, F., Luo, R., Dai, X., Liu, H., Yu, G., Han, S., Lu, X., Su, C., Chen, Q., Song, Q., et al. (2020). Chromosome-Level Reference Genome and Population Genomic Analysis Provide Insights into the Evolution and Improvement of Domesticated Mulberry (*Morus alba*). Molecular Plant *13*, 1001-1012. https://doi.org/10.1016/j.molp.2020.05.005.

39. Zhang, T., Liu, G., Zhao, H., Braz, G.T., and Jiang, J. (2021). Chorus2: design of genome-scale oligonucleotide-based probes for fluorescence in situ hybridization. Plant biotechnology journal *19*, 1967-1978. 10.1111/pbi.13610.

40. Zhou, Q.M., Li, J.C., Xuan, Y.H., Qiu, J.L., Yuan, J.L., Li, Z.A., Chen, S., and He, N.J. (2026). Precise identification of intersectional hybrids in *Morus* using genomic *in situ* hybridization (GISH). Forestry Research *6*, e010, e010. 10.48130/forres-0026-0009.

41. Xuan, Y.H., Li, C.S., Wu, Y., Ma, B., Liu, R.L., and He, N.J. (2017). FISH-based mitotic and meiotic diakinesis karyotypes of *Morus notabilis* reveal a chromosomal fusion-fission cycle between mitotic and meiotic phases. Scientific Reports *7*, 9573, 9573. 10.1038/s41598-017-10079-6.

42. Kolano, B., Tomczak, H., Molewska, R., Jellen, E.N., and Maluszynska, J. (2012). Distribution of 5S and 35S rRNA gene sites in 34 *Chenopodium* species (Amaranthaceae). Botanical Journal of the Linnean Society *170*, 220-231. 10.1111/j.1095-8339.2012.01286.x.

43. Zhao, Q.Z., Bai, Y.L., Wang, Y.H., Cheng, C.Y., Yu, X.Q., Lou, Q.F., and Chen, J.F. (2025). Chromosome-specific oligo-painting provides insights into the cytogenetic basis of karyotypic stasis in paleo-allotetraploid *Cucurbita*. Horticulture Research *12*, uhaf179, uhaf179. 10.1093/hr/uhaf179.

44. Ma, B., Wang, H., Liu, J., Chen, L., Xia, X., Wei, W., Yang, Z., Yuan, J., Luo, Y., and He, N. (2023). The gap-free genome of mulberry elucidates the architecture and evolution of polycentric chromosomes. Horticulture Research *10*, uhad111. 10.1093/hr/uhad111.

45. Yang, J., Peng, Y., Yang, F., Meng, G., and Kong, W. (2025). The telomere-to-telomere genome assembly of the wild mulberry, *Morus mongolica*. Scientific Data *12*, 694. 10.1038/s41597-025-05040-6.

46. Falistocco, E. (2009). Presence of triploid cytotypes in the common fig (*Ficus carica* L.). Genome *52*, 919-925. 10.1139/g09-068.

47. Ragone, D. (2001). Chromosome numbers and pollen stainability of three species of Pacific Island breadfruit (*Artocarpus,* Moraceae). American Journal of Botany *88*, 693-696. 10.2307/2657070.

48. Zerega, N., Wiesner-Hanks, T., Ragone, D., Irish, B., Scheffler, B., Simpson, S., and Zee, F. (2015). Diversity in the breadfruit complex (*Artocarpus*, Moraceae): genetic characterization of critical germplasm. Tree Genetics & Genomes *11*, 4, 4. 10.1007/s11295-014-0824-z.

49. Rizzon, C., Ponger, L., and Gaut, B.S. (2006). Striking similarities in the genomic distribution

of tandemly arrayed genes in *Arabidopsis* and rice. PLoS Computational Biology *2*, 989-1000, E115. 10.1371/journal.pcbi.0020115.

50. Rody, H.V.S., Baute, G.J., Rieseberg, L.H., and Oliveira, L.O. (2017). Both mechanism and age of duplications contribute to biased gene retention patterns in plants. BMC Genomics *18*, 46, 46. 10.1186/s12864-016-3423-6.

51. Almeida-Silva, F., and Van de Peer, Y. (2023). Whole-genome Duplications and the Long-term Evolution of Gene Regulatory Networks in Angiosperms. Molecular Biology and Evolution *40*, msad141, msad141. 10.1093/molbev/msad141.

52. Jiang, X., Hu, Q., Mei, D., Li, X., Xiang, L., Al-Shehbaz, I.A., Song, X., Liu, J., Lysak, M.A., and Sun, P. (2025). Chromosome fusions shaped karyotype evolution and evolutionary relationships in the model family Brassicaceae. Nature Communications *16*, 4631. 10.1038/s41467-025-59640-2.

53. Cheng, F., Wu, J., Cai, X., Liang, J.L., Freeling, M., and Wang, X.W. (2018). Gene retention, fractionation and subgenome differences in polyploid plants. Nature Plants *4*, 258-268. 10.1038/s41477-018-0136-7.

54. Ren, R., Wang, H.F., Guo, C.C., Zhang, N., Zeng, L.P., Chen, Y.M., Ma, H., and Qi, J. (2018). Widespread Whole Genome Duplications Contribute to Genome Complexity and Species Diversity in *Angiosperms*. Molecular Plant *11*, 414-428. 10.1016/j.molp.2018.01.002.

55. Zhang, K., Wang, X.W., and Cheng, F. (2019). Plant Polyploidy: Origin, Evolution, and Its Influence on Crop Domestication. Horticultural Plant Journal *5*, 231-239. 10.1016/j.hpj.2019.11.003.

56. Wang, Y.Y., Chen, B.H., Xiang, G.S., Wang, Y.N., Yang, R., Li, X.B., Yuan, S.Y., Zhao, Y.C., Zhang, G.H., Qin, M.J., and Yang, S.C. (2026). A Near Telomere-to-Telomere Genome of *Belamcanda chinensis* Provides Insights Into Genome Evolution and the Biosynthesis of Characteristic Isoflavones. Plant biotechnology journal *24*, 4285-4301. 10.1111/pbi.70612.

57. Chen, R., Meng, S.H., Wang, A.Q., Jiang, F., Yuan, L.H., Lei, L.H., Wang, H.C., and Fan, W. (2024). The genomes of seven economic Caesalpinioideae trees provide insights into polyploidization history and secondary metabolite biosynthesis. Plant communications *5*, 100944, 100944. 10.1016/j.xplc.2024.100944.

58. Huang, P., Li, Z., Wang, H., Huang, J.Q., Tan, G.F., Fu, Y., Liu, X.B., Zheng, S., Xu, P., Sun, M.S., and Zeng, J.G. (2024). A genome assembly of decaploid *Houttuynia cordata* provides insights into the evolution of *Houttuynia* and the biosynthesis of alkaloids. Horticulture Research *11*, uhae203, uhae203. 10.1093/hr/uhae203.

59. Zhang, Y., Ge, W.A., Teng, J., Yang, Y.M., Wang, J.Y., Yu, Z.J., Wang, J.Q., Xiao, Q.M., Zhao, J.X., Shen, S.Q., et al. (2024). Allotetraploidization event of *Coptis chinensis* shared by all Ranunculales. Horticultural Plant Journal *10*, 288-303. 10.1016/j.hpj.2023.01.004.

60. Wang, J.L., Song, B.W., Yang, M.R., Hu, F.B., Qi, H.L., Zhang, H.Z., Jia, Y.L., Li, Y.J., Wang, Z.Y., and Wang, X.Y. (2024). Deciphering recursive polyploidization in Lamiales and reconstructing their chromosome evolutionary trajectories. Plant Physiology *195*, 2143-2157. 10.1093/plphys/kiae151.

61. Zhang, J., Wang, D., Guo, G., Wang, S., Zhang, J., Liang, Y., Chen, F., and Wang, W. (2025). Genomic and metabolomic analysis of *Ficus altissima* and *Ficus hirta*: evolutionary divergence and medicinal implications. Tropical Plants *4*, e022. 10.48130/tp-0025-0014.

62. Kovalsky, I.E., and Solís Neffa, V.G. (2012). Evidence of 2*n* microspore production in a natural

diploid population of *Turnera sidoides* subsp. *carnea* and its relevance in the evolution of the *T. sidoides* (*Turneraceae*) autopolyploid complex. Journal of Plant Research *125*, 725-734. 10.1007/s10265-012-0493-7.

63. Kovalsky, I.E., and Solís Neffa, V.G. (2016). Evidence of the production of 2*n* eggs in diploid plants of the autopolyploid complex *Turnera sidoides* L. (Passifloraceae). Plant Systematics and Evolution *302*, 357-366. 10.1007/s00606-015-1268-0.

64. Bretagnolle, F., and Thompson, J.D. (1995). Gametes with the somatic chromosome number: mechanisms of their formation and role in the evolution of autopolyploid plants. New Phytologist *129*, 1-22. 10.1111/j.1469-8137.1995.tb03005.x.

65. den Nijs, T.P.M., and Peloquin, S.J. (1977). 2n gametes in potato species and their function in sexual polyploidization. Euphytica *26*, 585-600. 10.1007/BF00021684.

66. Addo Nyarko, C., Katche, E., Báez, M., Lv, Z., and Mason, A.S. (2025). A wide range of chromosome numbers result from unreduced gamete production in *Brassica juncea* × *B. napus* (AABC) interspecific hybrids. Heredity *134*, 98-108. 10.1038/s41437-024-00738-6.

67. Mandáková, T., and Lysak, M.A. (2018). Post-polyploid diploidization and diversification through dysploid changes. Current Opinion in Plant Biology *42*, 55-65. 10.1016/j.pbi.2018.03.001.

68. Ma, X.F., and Gustafson, J.P. (2005). Genome evolution of allopolyploids: a process of cytological and genetic diploidization. Cytogenetic and Genome Research *109*, 236-249. 10.1159/000082406.

69. Mandáková, T., Li, Z., Barker, M.S., and Lysak, M.A. (2017). Diverse genome organization following 13 independent mesopolyploid events in *Brassicaceae* contrasts with convergent patterns of gene retention. Plant Journal *91*, 3-21. 10.1111/tpj.13553.

70. Li, Z., McKibben, M.T.W., Finch, G.S., Blischak, P.D., Sutherland, B.L., and Barker, M.S. (2021). Patterns and Processes of Diploidization in Land Plants. Annual Review of Plant Biology *72*, 387-410. 10.1146/annurev-arplant-050718-100344.

71. Wang, X.Y., Jin, D.C., Wang, Z.Y., Guo, H., Zhang, L., Wang, L., Li, J.P., and Paterson, A.H. (2015). Telomere-centric genome repatterning determines recurring chromosome number reductions during the evolution of eukaryotes. New Phytologist *205*, 378-389. 10.1111/nph.12985.

72. Li, Z.F., Zhu, Z.Y., Qian, K., Tang, B.P., Han, B.C., Zhong, Z.H., Fu, T., Zhou, P., Stukenbrock, E.H., Martin, F.M., and Yuan, Z.L. (2024). Intraspecific diploidization of a halophyte root fungus drives heterosis. Nature Communications *15*, 5872, 5872. 10.1038/s41467-024-49468-7.

73. Mandáková, T., Guo, X.Y., Özüdogru, B., Mummenhoff, K., and Lysak, M.A. (2018). Hybridization-facilitated genome merger and repeated chromosome fusion after 8 million years. Plant Journal *96*, 748-760. 10.1111/tpj.14065.

74. Yu, Z.H., Huang, Y.J., Yu, X.K., Deng, Z.H., Chai, J., Liu, J.R., Gong, Z.Y., Yao, W., Zhang, J.S., Zhang, M.Q., et al. (2025). Formation and centromere inactivation of fusion chromosomes in two allotetraploid species from the *Saccharum* complex. New Phytologist *247*, 2697-2708. 10.1111/nph.70369.

75. Huang, Y., Poretti, M., Mandáková, T., Pouch, M., Guo, X., Anani, H., Perez-Roman, E., Crespo, M.B., Grob, S., Bousios, A., et al. (2026). Post-polyploid chromosomal diploidization in plants is affected by clade divergence and constrained by shared genomic features. Nature

Communications. 10.1038/s41467-026-73793-8.
76. Xie, C., Ma, Z., Zhou, C., Ma, K., Wang, H., Wu, J., Zhou, Y., Lu, Y., Ji, D., Gu, X., et al. (2026). Chromosomal fusions trigger rediploidization of autopolyploid genomes. Nature *654*, 706-713. 10.1038/s41586-026-10439-1.
77. Xia, Z.Q., Dai, X.L., Fan, W., Liu, C.Y., Zhang, M.R., Bian, P.P., Zhou, Y.P., Li, L., Zhu, B.Z., Liu, S.M., et al. (2022). Chromosome-level Genomes Reveal the Genetic Basis of Descending Dysploidy and Sex Determination in *Morus* Plants. Genomics Proteomics & Bioinformatics *20*, 1119-1137. 10.1016/j.gpb.2022.08.005.
78. Mata-Sucre, Y., Krátká, M., Oliveira, L., Neumann, P., Macas, J., Schubert, V., Huettel, B., Kejnovský, E., Houben, A., Pedrosa-Harand, A., et al. (2024). Repeat-based holocentromeres of the woodrush *Luzula sylvatica* reveal insights into the evolutionary transition to holocentricity. Nature Communications *15*, 9565. 10.1038/s41467-024-53944-5.
79. Shao, Y.Y., Lu, N., Wu, Z.F., Cai, C., Wang, S.S., Zhang, L.L., Zhou, F., Xiao, S.J., Liu, L., Zeng, X.F., et al. (2018). Creating a functional single-chromosome yeast. Nature *560*, 331-335. 10.1038/s41586-018-0382-x.
80. Luo, J.C., Sun, X.J., Cormack, B.P., and Boeke, J.D. (2018). Karyotype engineering by chromosome fusion leads to reproductive isolation in yeast. Nature *560*, 392-396. 10.1038/s41586-018-0374-x.
81. Murat, F., Zhang, R., Guizard, S., Gavranović, H., Flores, R., Steinbach, D., Quesneville, H., Tannier, E., and Salse, J. (2015). Karyotype and Gene Order Evolution from Reconstructed Extinct Ancestors Highlight Contrasts in Genome Plasticity of Modern Rosid Crops. Genome Biology and Evolution *7*, 735-749. 10.1093/gbe/evv014 %J Genome Biology and Evolution.
82. Pont, C., Wagner, S., Kremer, A., Orlando, L., Plomion, C., and Salse, J. (2019). Paleogenomics: reconstruction of plant evolutionary trajectories from modern and ancient DNA. Genome Biology *20*, 29. 10.1186/s13059-019-1627-1.
83. Liu, J., Zhou, S.-Z., Liu, Y.-L., Zhao, B.-Y., Yu, D., Zhong, M.-C., Jiang, X.-D., Cui, W.-H., Zhao, J.-X., Qiu, J., et al. (2024). Genomes of *Meniocus linifolius* and *Tetracme quadricornis* reveal the ancestral karyotype and genomic features of core Brassicaceae. Plant communications *5*, 100878. https://doi.org/10.1016/j.xplc.2024.100878.
84. Stai, J.S., Cardinal-McTeague, W., Bruneau, A., and Cannon, S.B. (2026). Complex reticulation in backbone subfamily relationships in Leguminosae. Molecular Phylogenetics and Evolution *214*, 108438. https://doi.org/10.1016/j.ympev.2025.108438.
85. Chen, F., Su, L., Hu, S., Xue, J.-Y., Liu, H., Liu, G., Jiang, Y., Du, J., Qiao, Y., Fan, Y., et al. (2021). A chromosome-level genome assembly of rugged rose (*Rosa rugosa*) provides insights into its evolution, ecology, and floral characteristics. Horticulture Research *8*, 141. 10.1038/s41438-021-00594-z.
86. Xin, H., Wang, Y., Li, Q., Wan, T., Hou, Y., Liu, Y., Gichuki, D.K., Zhou, H., Zhu, Z., Xu, C., et al. (2022). A genome for *Cissus* illustrates features underlying its evolutionary success in dry savannas. Horticulture Research *9*, uhac208. 10.1093/hr/uhac208.
87. Xiao, P.X., Li, Y., Lu, J., Zuo, H., Pingcuo, G., Ying, H., Zhao, F., Xu, Q., Zeng, X., and Jiao, W.B. (2023). High-quality assembly and methylome of a Tibetan wild tree peony genome (*Paeonia ludlowii*) reveal the evolution of giant genome architecture. Horticulture Research *10*, uhad241. 10.1093/hr/uhad241.
88. Wang, X., Sun, J., Wang, J., Zhang, X., Chen, S., Jin, J., Zhang, X., Khan, F.S., Wang, K., Mei,

J., et al. (2026). Chromosome-level phylogenomics and genome evolution of the grape family. Nature Plants *12*, 2358-2376. 10.1038/s41477-026-02442-1.

89. Albert, P.S., Zhang, T., Semrau, K., Rouillard, J.M., Kao, Y.H., Wang, C.J.R., Danilova, T.V., Jiang, J.M., and Birchler, J.A. (2019). Whole-chromosome paints in maize reveal rearrangements, nuclear domains, and chromosomal relationships. Proceedings of the National Academy of Sciences *116*, 1679-1685. 10.1073/pnas.1813957116.
90. Shi, P.Y., Sun, H.J., Liu, G.Q., Zhang, X., Zhou, J.W., Song, R.R., Xiao, J., Yuan, C.X., Sun, L., Wang, Z.K., et al. (2022). Chromosome painting reveals inter-chromosomal rearrangements and evolution of subgenome D of wheat. Plant Journal *112*, 55-67. 10.1111/tpj.15926.
91. Zhao, Q.Z., Meng, Y., Wang, P.Q., Qin, X.D., Cheng, C.Y., Zhou, J.G., Yu, X.Q., Li, J., Lou, Q.F., Jahn, M., and Chen, J.F. (2021). Reconstruction of ancestral karyotype illuminates chromosome evolution in the genus *Cucumis*. Plant Journal *107*, 1243-1259. 10.1111/tpj.15381.
92. Meng, Z., Zheng, Q., Shi, S.D., Wang, W., Wang, F., Xie, Q.L., Chen, X.F., Shen, H.T., Xiao, G.H., and Li, H.B. (2024). Whole-chromosome oligo-painting in licorice unveils interspecific chromosomal evolutionary relationships and possible origin of triploid genome species. Plant Journal *120*, 2089-2100. 10.1111/tpj.17102.
93. Qu, M.M., Zhang, L.Y., Li, K.P., Sun, J.Y., Li, Z.Y., and Han, Y.H. (2021). Karyotypic stability of *Fragaria* (strawberry) species revealed by cross-species chromosome painting. Chromosome Research *29*, 285-300. 10.1007/s10577-021-09666-1.
94. Jiménez-Martín, A., Pineda-Santaella, A., Martín-García, R., Esteban-Villafañe, R., Matarrese, A., Pinto-Cruz, J., Camacho-Cabañas, S., León-Periñán, D., Terrizzano, A., Daga, R.R., et al. (2025). Centromere positioning orchestrates telomere bouquet formation and the initiation of meiotic differentiation. Nature Communications *16*, 837. 10.1038/s41467-025-56049-9.
95. Lysak, M.A. (2022). Celebrating Mendel, McClintock, and Darlington: On end-to-end chromosome fusions and nested chromosome fusions. The Plant cell *34*, 2475-2491. 10.1093/plcell/koac116.
96. Vozárová, R., Wang, W.C., Lunerová, J., Shao, F.Q., Pellicer, J., Leitch, I.J., Leitch, A.R., and Kovarík, A. (2022). Mega-sized pericentromeric blocks of simple telomeric repeats and their variants reveal patterns of chromosome evolution in ancient Cycadales genomes. Plant Journal *112*, 646-663. 10.1111/tpj.15969.
97. Ma, Y., Zhao, X., Jia, Y., Han, Z., Yu, C., Fan, Z., Zhang, Z., Xiao, J., Zhao, W., Bao, Y., and Chen, M. (2025). The Updated Genome Warehouse: Enhancing Data Value, Security, and Usability to Address Data Expansion. Genomics Proteomics & Bioinformatics *23*, qzaf010. 10.1093/gpbjnl/qzaf010.
98. Partners, C.N.M.a. (2026). Database resources of the National Genomics Data Center, China National Center for Bioinformation in 2026. Nucleic acids research *54*, D28-D47. 10.1093/nar/gkaf1172.
99. Bi, Y.F., Zhao, Q.Z., Yan, W.K., Li, M.X., Liu, Y.X., Cheng, C.Y., Zhang, L., Yu, X.Q., Li, J., Qian, C.T., et al. (2020). Flexible chromosome painting based on multiplex PCR of oligonucleotides and its application for comparative chromosome analyses in *Cucumis*. Plant Journal *102*, 178-186. 10.1111/tpj.14600.
100. Benson, G. (1999). Tandem repeats finder: a program to analyze DNA sequences. Nucleic acids research *27*, 573-580. 10.1093/nar/27.2.573.
101. Jiang, C., Liu, X., Yang, Z., and Li, G. (2023). Chromosome Rearrangement in *Elymus*

dahuricus Revealed by ND-FISH and Oligo-FISH Painting. Plants *12*, 3268. 10.3390/plants12183268.

102. Huang, H., Zhang, T., Sun, P., Chen, Y., Zhao, D., Zhang, X., and Ma, H. (2026). A high-quality chromosome-level genome assembly of *Ficus carica* cultivar 'Green Peel'. Scientific Data *13*, 1390. 10.1038/s41597-026-07646-w.

103. Xia, Z.Q., Fan, W., Liu, D.Y., Chen, Y.E., Lv, J., Xu, M.X., Zhang, M.R., Ren, Z.Z., Chen, X.F., Wang, X.J., et al. (2024). Haplotype-resolved chromosomal-level genome assembly reveals regulatory variations in mulberry fruit anthocyanin content. Horticulture Research *11*, uhae120, uhae120. 10.1093/hr/uhae120.

104. Sun, P.C., Jiao, B.B., Yang, Y.Z., Shan, L.X., Li, T., Li, X.N., Xi, Z.X., Wang, X.Y., and Liu, J.Q. (2022). WGDI: A user-friendly toolkit for evolutionary analyses of whole-genome duplications and ancestral karyotypes. Molecular Plant *15*, 1841-1851. 10.1016/j.molp.2022.10.018.

105. Dai, F.W., Zhuo, X.K., Luo, G.Q., Wang, Z.J., Xu, Y.J., Wang, D., Zhong, J.W., Lin, S., Chen, L., Li, Z.Y., et al. (2023). Genomic Resequencing Unravels the Genetic Basis of Domestication, Expansion, and Trait Improvement in *Morus Atropurpurea*. Advanced Science *10*, 2300039. 10.1002/advs.202300039.

106. Scrucca, L., Fraley, C., Murphy, T.B., Raftery, A.E.J.M.-B.C., Classification,, and R, D.E.U.m.i. (2023). Model-Based Clustering, Classification, and Density Estimation Using mclust in R. Chapman & Hall/CRC. https://mclust-org.github.io/book/.

107. Pérez-Wohlfeil, E., Diaz-del-Pino, S., and Trelles, O. (2019). Ultra-fast genome comparison for large-scale genomic experiments. Scientific Reports *9*, 10274, 10274. 10.1038/s41598-019-46773-w.

108. Liao, S., Zhang, Z., Yang, C.X., Gardner, E.M., Peng, Y.Q., Xiong, Y.M., Dai, S.P., and Deng, Y.F. (2025). A chromosome-level genome assembly of *Ficus benjamina*, a fig tree with great ecological and ornamental value. Scientific Data *12*, 824, 824. 10.1038/s41597-025-05155-w.

109. Jia, X.W., Li, H.Y., Han, Y., Wang, L., Lai, C.J., Liu, X., Li, P., Lei, Z.P., and Zhang, Y.H. (2025). Genome-wide microsatellite characterization and their marker development and transferability in *Broussonetia* Species. BMC Genomics *26*, 61, 61. 10.1186/s12864-025-11238-0.

110. Huang, W.C., Ding, Y.M., Fan, S.L., Liu, W.Z., Chen, H.F., Segar, S., Compton, S.G., and Yu, H. (2024). A high-quality chromosome-level genome assembly of *Ficus hirta*. Scientific Data *11*, 526, 526. 10.1038/s41597-024-03376-z.

111. Miao, K., Wang, Y., Hou, L.X., Liu, Y., Liu, H.Y., and Ji, Y.H. (2024). Haplotype-resolved genome assembly of the upas tree (*Antiaris toxicaria*). Scientific Data *11*, 1011. 10.1038/s41597-024-03860-6.

112. Marçais, G., Delcher, A.L., Phillippy, A.M., Coston, R., Salzberg, S.L., and Zimin, A. (2018). MUMmer4: A fast and versatile genome alignment system. PLoS Computational Biology *14*, e1005944, e1005944. 10.1371/journal.pcbi.1005944.

113. Sun, P., Lu, Z., Wang, Z., Wang, S., Zhao, K., Mei, D., Yang, J., Yang, Y., Renner, S.S., and Liu, J. (2024). Subgenome-aware analyses reveal the genomic consequences of ancient allopolyploid hybridizations throughout the cotton family. Proceedings of the National Academy of Sciences *121*, e2313921121. doi:10.1073/pnas.2313921121.

114. Buchfink, B., Xie, C., and Huson, D.H. (2015). Fast and sensitive protein alignment using DIAMOND. Nature Methods *12*, 59-60. 10.1038/nmeth.3176.

115. He, J., Bao, S., Deng, J., Li, Q., Ma, S., Liu, Y., Cui, Y., Zhu, Y., Wei, X., Ding, X., et al. (2022). A chromosome-level genome assembly of *Artocarpus nanchuanensis* (Moraceae), an extremely endangered fruit tree. GigaScience *11*, giac042. 10.1093/gigascience/giac042.